© 2020. Published by The Company of Biologists Ltd | Development (2020) 147, dev195941. doi:10.1242/dev.195941

RESEARCH ARTICLE

Negative feedback by conserved kinases patterns the degradation of *Caenorhabditis elegans* Raf in vulval fate patterning

Claire C. de la Cova[1,2,*,‡], Robert Townley[1,2,*] and Iva Greenwald[1]

ABSTRACT

Activation of a canonical EGFR-Ras-Raf-ERK cascade initiates patterning of multipotent vulval precursor cells (VPCs) of *Caenorhabditis elegans*. We have previously shown that this pathway includes a negative-feedback component in which MPK-1/ERK activity targets the upstream kinase LIN-45/Raf for degradation by the SEL-10/FBXW7 E3 ubiquitin ligase. This regulation requires a Cdc4 phosphodegron (CPD) in LIN-45 that is conserved in BRAF. Here, we identify and characterize the minimal degron that encompasses the CPD and is sufficient for SEL-10-mediated, MPK-1-dependent protein degradation. A targeted screen of conserved protein kinase-encoding genes yielded *gsk-3* (an ortholog of human GSK3B) and *cdk-2* (a CDK2-related kinase) as required for LIN-45 degron-mediated turnover. Genetic analysis revealed that LIN-45 degradation is blocked at the second larval stage due to cell cycle quiescence, and that relief of this block during the third larval stage relies on activation of CDKs. Additionally, activation of MPK-1 provides spatial pattern to LIN-45 degradation but does not bypass the requirement for *gsk-3* and *cdk-2*. This analysis supports a model whereby MPK-1/ERK, GSK-3/GSK3 and CDK-2/CDK2, along with SEL-10/FBXW7, constitute a regulatory network that exerts spatial and temporal control of LIN-45/Raf degradation during VPC patterning.

KEY WORDS: Cdc4 phosphodegron, LIN-45/BRAF, Negative feedback, Protein degradation, Raf-MEK-ERK, SEL-10/FBXW7

INTRODUCTION

Genetic analysis of *Caenorhabditis elegans* vulval cell fate patterning has provided many insights into EGF receptor (EGFR) signal transduction and its regulation (Gauthier and Rocheleau, 2017; Shin and Reiner, 2018; Sternberg, 2005; Sundaram, 2013). Six multipotential vulval precursor cells (VPCs), designated P3.p to P8.p, have the potential to adopt one of three fates, termed primary, secondary or tertiary (Fig. 1A). Normally, an EGF-like inductive signal from the anchor cell (AC) of the gonad initiates pattern formation by activating LET-23/EGFR and a canonical Ras-Raf-ERK cascade in P6.p, the VPC nearest the AC. Activated ERK in P6.p promotes the primary fate and the production of Delta/Serrate/LAG-2 (DSL) ligands that activate LIN-12/Notch in the flanking VPCs, P5.p and P7.p, specifying them to adopt the secondary fate. The outer VPCs, in which neither EGFR nor Notch is active, adopt the tertiary fate and do not contribute to the vulva. This apparently simple fate pattern is invariant, precise and robust, because many different regulatory mechanisms ensure appropriate initiation, intensity, duration and integration of these LET-23/EGFR- and LIN-12/Notch-mediated signaling events.

Signal transduction by EGFR occurs via LET-60/Ras and a conserved kinase cascade composed of LIN-45/Raf, MEK-2/MEK and MPK-1/ERK (Gauthier and Rocheleau, 2017; Shin and Reiner, 2018; Sternberg, 2005; Sundaram, 2013). In this study, we investigate a negative-feedback mechanism in which high MPK-1 activity in P6.p leads to degradation of LIN-45 (de la Cova and Greenwald, 2012; see also Fig. 1B). We originally identified this negative regulatory mechanism via a computational search for potential substrates of SEL-10/FBXW7, a highly conserved substrate-recognition subunit of a multiprotein Skp-Cullin-F-box (SCF) E3 ubiquitin ligase and a commonly mutated tumor suppressor gene (Yumimoto and Nakayama, 2020). FBXW7 substrates contain a sequence called a 'CPD' (Cdc4 phosphodegron) that, when phosphorylated at two key residues, acts as a high-affinity binding site for FBXW7, thereby targeting that substrate for ubiquitin-mediated degradation (Nash et al., 2001; Orlicky et al., 2003). We found that LIN-45 has a CPD consensus sequence that is conserved in mammalian BRAF (de la Cova and Greenwald, 2012; see also Fig. 1C). By examining the consequences for stability and activity of LIN-45 when the CPD is mutated, and in mutants lacking *sel-10*, we validated LIN-45 as a SEL-10 substrate. In VPCs, LIN-45 protein degradation requires MPK-1 activity and occurs specifically in P6.p, where MPK-1 activation is highest (Fig. 1A). This negative-feedback mechanism also appears to operate in mammalian cells (see Discussion).

There is also a temporal dimension to cell fate specification of the multipotent VPCs. They are born in the first larval (L1) stage, and remain in a G0/G1-like cell cycle phase throughout the second larval (L2) stage (Ambros, 1999; Euling and Ambros, 1996; Hong et al., 1998). EGFR signal transduction in P6.p begins soon after entry into the L2 stage (de la Cova et al., 2017), but VPC fates are not fixed until later, in the third larval (L3) stage (Ferguson et al., 1987; Greenwald et al., 1983; Sternberg and Horvitz, 1986). Maintenance of cell cycle quiescence during L2 is controlled by 'heterochronic' genes (Euling and Ambros, 1996; Hong et al., 1998) that allow expression of genes that inhibit cell cycle cyclin-dependent kinases (CDKs) (Buck et al., 2009; Saito et al., 2004). In the early L3 stage, VPCs enter S phase and divide in the mid-L3 stage (Ambros, 1999; Sulston and Horvitz, 1977). Hydroxyurea (HU) blockade of S phase reveals that P6.p is committed to the primary fate prior to DNA replication (Ambros, 1999; Euling and Ambros, 1996; Hong et al., 1998), implying coordination between the cell cycle and VPC fate specification.

[1]Department of Biological Sciences, Columbia University, New York, NY 10027, USA. [2]Department of Biological Sciences, University of Wisconsin Milwaukee, Milwaukee, WI 53201, USA.
*Present address: Department of Biological Sciences, University of Wisconsin Milwaukee, Milwaukee, WI 53201.

‡Author for correspondence (delacova@uwm.edu)

C.C.d.l.C., 0000-0001-8719-6883

Handling Editor: Thomas Lecuit
Received 12 August 2020; Accepted 27 October 2020

Development (2020) 147, dev195941. doi:10.1242/dev.195941

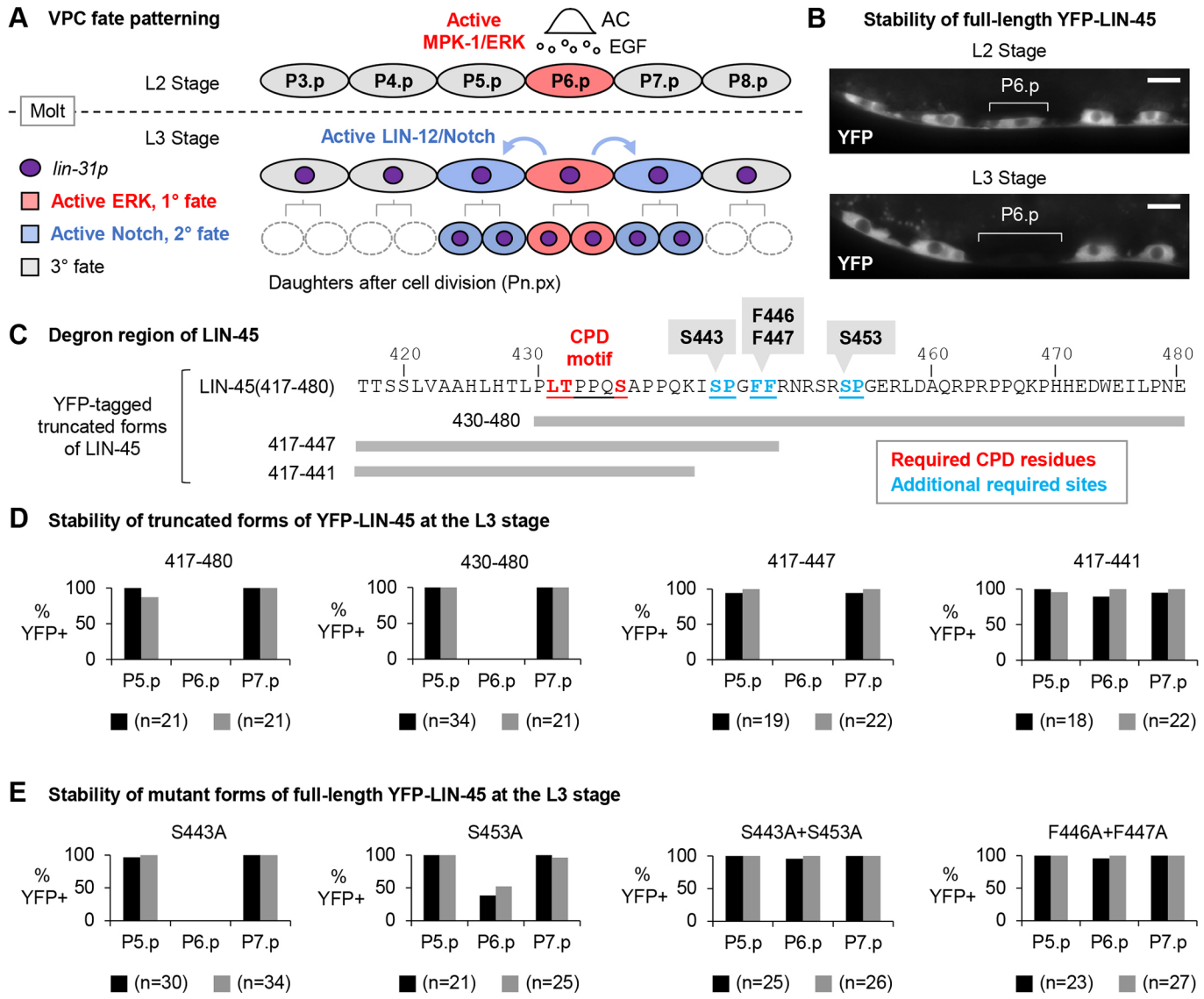

Fig. 1. Identification and characterization of the LIN-45 degron. (A) VPC fate patterning. In the L2 stage, VPCs remain multipotent and in a G0/G1-like cell cycle phase; they proceed into S phase in the early L3 stage. An EGF-like ligand produced in the anchor cell (AC) activates an EGFR-Ras-ERK cascade in P6.p in the early L2 stage. However, P6.p does not commit to the primary (1°) fate until the early L3 stage. Descendants of P6.p (primary fate), and P5.p and P7.p (secondary fate, 2°), form the vulva, and the daughters of tertiary (3°) VPCs fuse with the major hypodermal syncytium, indicated by dashed cell outlines. After cell division, daughters of VPCs are collectively termed Pn.px. (B) When *lin-31p* is used to drive full-length YFP-tagged LIN-45 (YFP-LIN-45), YFP is visible in all VPCs throughout the L2 stage (top) and is degraded in P6.p at the L3 stage (bottom). Scale bar: 10 µm. (C) The degron region of LIN-45. Truncated regions used to make YFP-tagged reporters, required CPD residues (red) and potential S-P phosphorylation sites and phenylalanine residues (blue) mutated in this study are indicated. (D,E) For all experiments with the indicated truncated or mutated forms of YFP-LIN-45, two independent transgenes were assessed; data for the two are shown in black and gray columns in every graph. For each transgene, the percentage of VPCs positive for YFP and the number of larvae scored (*n*) is shown. Daughters of P5.p, P6.p, and P7.p were scored to ensure that signaling events that specify cell fate had occurred. (D) The YFP-LIN-45(417-480) reporter displays the same patterned degradation as full-length LIN-45. (E) Degradation of the full-length YFP-LIN-45 requires sites at S443, S453, and F446/F447.

SEL-10-mediated LIN-45 protein degradation in P6.p also occurs in the L3 stage, coincident with the time of commitment to the primary fate, rather than earlier in response to MPK-1 activation during the L2 stage. This timing suggests that LIN-45 degradation is temporally gated and requires more than just MPK-1 activation, and also raises the question of how the onset of negative feedback is coordinated with developmental timing. To understand this at a mechanistic level, we turned to analysis of the LIN-45 CPD. For all known SEL-10/FBXW7 substrates, high-affinity binding requires phosphorylation of two specific residues, a 'central threonine' (referred to throughout as +0 Thr) and a serine at position +4 relative to the +0 Thr (+4 Ser) of the substrate CPD. The analysis presented here implicates two potential proline-directed phosphorylation sites near the CPD that are required for degradation, suggesting that phosphorylation at sites other than the +0 Thr and +4 Ser residues impinges on SEL-10-dependent degradation. We also performed a targeted RNAi screen of the 248 *C. elegans* protein kinase-encoding genes that have human orthologs (Deng et al., 2019; Kim et al., 2018) and identified two kinases – GSK-3 and CDK-2 – that, in addition to MPK-1, are required for LIN-45 degradation in P6.p. Using different forms of LIN-45 and an *in vivo* biosensor to quantify MPK-1 activity, we analyzed the roles of GSK-3 and CDK-2 in restraining Raf-MEK-ERK signalling and identified a temporal block that prevents LIN-45 degradation in the L2 stage due to cell

Development (2020) 147, dev195941. doi:10.1242/dev.195941

cycle quiescence, which is relieved during the L3 stage by activation of CDKs. We propose a model wherein negative feedback acting on Raf-MEK-ERK signal transduction in VPCs is imposed by kinase-regulated protein degradation of LIN-45, with spatial and temporal patterning provided by MPK-1 and CDK-2.

RESULTS

Potential phosphorylation sites outside of the CPD are required for P6.p-specific degradation of full-length LIN-45

To define sequences that regulate LIN-45 degradation in *cis*, we created single-copy transgenes that express wild-type, truncated or mutant forms of yellow fluorescent protein (YFP)-tagged LIN-45 under the control of transcriptional regulatory sequences from *lin-31*, referred to here as *lin-31p* (Tan et al., 1998; see Materials and Methods). This method enables approximately uniform expression in all six VPCs from the early L2 stage and after VPCs divide in the L3 stage (de la Cova and Greenwald, 2012; see Fig. 1A), allowing us to focus on protein stability. When YFP-tagged wild-type LIN-45 (YFP-LIN-45) is expressed using *lin-31p*, it is stable in all VPCs at the L2 stage and degraded in P6.p prior to cell division (Fig. 1B). Degradation in P6.p depends on *sel-10* and *mpk-1* and the presence of the +0 Thr and +4 Ser phospho-acceptor sites of the CPD (Fig. 1C; de la Cova and Greenwald, 2012), consistent with the sequence requirements of high-affinity CPDs (Nash et al., 2001).

We previously showed that a 262-amino-acid region of LIN-45 lacking domains for Ras binding, kinase activity and dimerization, termed LIN-45(218-480), is sufficient to promote degradation in P6.p (de la Cova and Greenwald, 2012). To further define sequence requirements for degradation, we first analyzed YFP-LIN-45(417-480), which encompasses the CPD. This fragment was efficiently targeted for degradation (Fig. 1C,D, see also Fig. 2B), and the CPD +0 Thr and +4 Ser were required (Fig. S1), indicating that it contains the LIN-45 degron required for SEL-10-mediated negative feedback. A shorter derivative lacking sequences N-terminal to the CPD, YFP-LIN-45(430-480), was also robustly degraded in P6.p (Fig. 1D), so we focused on mutating residues C-terminal to the CPD to identify other potentially important sites for LIN-45 degron function (Fig. 1D; Fig. S1). Deletion of a C-terminal region with two potential Ser-Pro (S-P) sites at S443 and S453 resulted in stabilization of the YFP reporter in P6.p (Fig. 1D).

To test whether S443 and S453 act to promote LIN-45 degradation, we mutated them individually or together in the full-length YFP-LIN-45 context (Fig. 1E) and found that they act redundantly, because only the double mutant S443A+S453A was strongly stabilized in P6.p. Both are S-P sites, suggesting that regulation of LIN-45 stability may occur via a proline-directed kinase. Mutation of F446 and F447 to alanine also resulted in stabilization in P6.p (Fig. 1E), suggesting that they are required for an additional protein-protein interaction or conformation required for LIN-45 degradation; we did not study this site further, but it is tempting to speculate that these residues are part of a binding site for one or both of the kinases we identified below.

We note that we previously proposed that amino acids H426 to L431 of LIN-45 function as an MPK-1 docking site, because this region resembles a 'D domain'-type ERK docking site consensus (Biondi and Nebreda, 2003); we also provided support for this proposal by mutating L429 and L431, and found that alanine substitutions at these sites stabilize full-length LIN-45 (de la Cova and Greenwald, 2012). The observation here that YFP-LIN-45(430-480) retains degron function suggests that this sequence does not function as an MPK-1 docking site. Subsequent to our previous observations, it has been reported that FBXW7 substrate binding requires the '−1 leucine' residue, which corresponds to L429 in LIN-45 (Welcker et al., 2013). Thus, we now believe that the L429A+L431A mutations stabilized LIN-45 because CPD function was compromised, rather than because MPK-1 docking site function was eliminated.

An RNAi screen identifies GSK-3 and CDK-2 as negative regulators of LIN-45 stability

The presence of a phospho-regulated CPD and requirement for additional S-P sites in the LIN-45 degron suggested that protein kinases regulate LIN-45 protein stability. We performed an RNAi screen of the 248 kinases conserved between *C. elegans* and humans (Deng et al., 2019; Materials and Methods) for their ability to stabilize the truncated reporter YFP-LIN-45(417-480), a form that was brightly and reliably expressed in VPCs, and robustly degraded in P6.p (Fig. 1D). This screen identified two proline-directed kinases, GSK-3 and CDK-2, as required for YFP-LIN-45 degradation in P6.p in L3 stage larvae. To confirm the RNAi results, and for further analysis, we obtained *gsk-3(tm2223)* and *cdk-2(tm2244)* mutants [referred to hereafter as *gsk-3(0)* and *cdk-2(0)*, respectively], both of which have large deletions and are predicted null alleles. Here and below, we included the reporter *arIs222[lag-2p::2×NLS-tagRFP]* (Sallee and Greenwald, 2015); because *lag-2* expression in P6.p results from MPK-1-mediated phosphorylation of LIN-1/Elk1 (Jacobs et al., 1998; Underwood et al., 2017; Zhang and Greenwald, 2011). Expression of this RFP marker indicated that P6.p was appropriately induced by the inductive signal in the individuals we scored.

GSK-3, the ortholog of human GSK3B (glycogen synthase kinase 3 beta), acts in many cell processes and signal transduction pathways (Cohen and Frame, 2001). In contrast to wild-type L3 stage larvae (Fig. 2A,B), in *gsk-3(0)* mutants, YFP-LIN-45 protein was not degraded and was still present in P6.p (Fig. 2A,C). A transgene in which *lin-31p* drives expression of wild-type *gsk-3(+)* specifically in VPCs [*lin-31p::gsk-3(+)*] significantly restored YFP-LIN-45 degradation in *gsk-3(0)* mutants (Fig. 2C), consistent with a role for GSK-3 in the VPCs.

CDK-2 is a cyclin-dependent kinase related to the human cell cycle kinases CDK2, CDK1 and CDK3 (Kim et al., 2018), with functional similarities to the G1-to-S-promoting kinase CDK2 (Fox et al., 2011; Korzelius et al., 2011). In *cdk-2(0)* mutant L3 stage larvae, YFP-LIN-45 protein was not degraded in P6.p (Fig. 2A,D). Similarly, *cye-1(ar95)*, a null allele of cyclin E (Fay and Han, 2000) referred to here as *cye-1(0)*, also abrogated YFP-LIN-45 degradation (Fig. 2E). Expression of wild-type *cye-1(+)* in VPCs [*lin-31p::cye-1(+)*] significantly rescued YFP-LIN-45 degradation in the *cye-1(0)* background (Fig. 2E), supporting a role for CDK2 and cyclin E in VPCs.

CDK-2 and CYE-1 promote progression through the S phase of the cell cycle (Kipreos and van den Heuvel, 2019), raising the question of whether failure to degrade LIN-45 in the mutants resulted from failure of cell cycle progression. However, VPCs of *cdk-2(0)* and *cye-1(0)* mutants were capable of cell divisions (Fig. 2A) (Fay and Han, 2000), suggesting that CDK2-mediated LIN-45 degradation is not inextricably coupled to cell division. This conclusion was further supported by using HU to block S-phase progression and observing that YFP-LIN-45(417-480) was not stabilized (Fig. S2), indicating that CDK2 promotes degradation of LIN-45 independently of its role in promoting cell cycle progression.

Development (2020) 147, dev195941. doi:10.1242/dev.195941

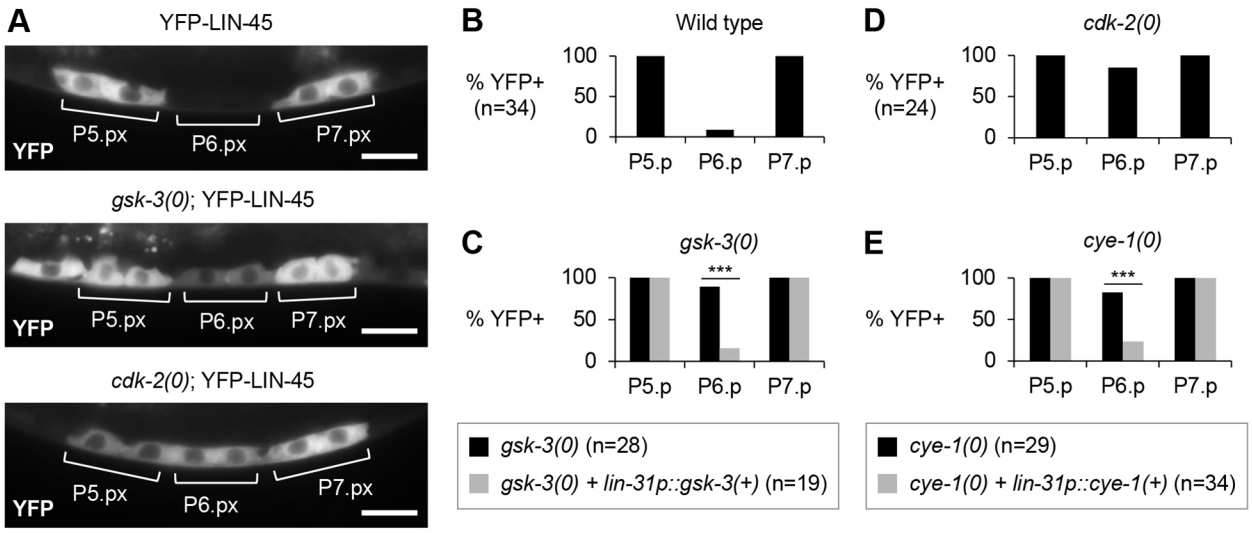

Fig. 2. GSK-3, CDK-2 and cyclin E are required for LIN-45 protein degradation in P6.p. (A) Stability of full-length YFP-LIN-45 in daughters of P5.p, P6.p, and P7.p (P5.px, P6.px and P7.px, respectively). Wild-type (top), *gsk-3(0)* mutant (center) and *cdk-2(0)* mutant (bottom) L3 stage larvae expressing YFP-LIN-45 are shown. Scale bar: 10 µm. (B-E) The percentage of VPCs positive for YFP-LIN-45 and number of larvae scored (*n*) are shown for: (B) wild type, (C) *gsk-3(0)* and *gsk-3(0) arTi129[lin-31p::gsk-3(+)]*, (D) *cdk-2(0)*, (E) *cye-1(0),* and *cye-1(0) arTi7[lin-31p::cye-1(+)]*. Daughters of P5.p, P6.p and P7.p were scored in these experiments to ensure that signaling events that specify cell fate had occurred. All data shown is from larvae in which P6.p daughters were positive for tagRFP expression from the *arIs222[lag-2p::2×NLS-tagRFP]* reporter, an indication that Ras-Raf-ERK signal transduction and primary cell fate induction had occurred. A two-tailed Fisher's exact test was performed to compare the numbers of YFP-positive P6.p cells. *gsk-3(0)* mutants were compared with *gsk-3(0)+lin-31p::gsk-3(+)*; *cye-1(0)* mutants were compared with *cye-1(0)+lin31p::cye-1(+)*. ***P<0.0001.

Loss of either GSK-3 or CDK-2 enhances LIN-45(V627E) activity in VPCs

We next assessed the effect of *gsk-3(0)* and *cdk-2(0)* on LIN-45 biological activity, using cell fate as a readout. In wild-type larvae, VPCs that do not receive EGFR- or Notch-mediated inputs (P3.p, P4.p and P8.p) adopt the tertiary (non-vulval) fate (Fig. 1A). Mutations that increase Ras-Raf-ERK pathway activity cause these cells to behave as if they have received EGF and to adopt the primary fate. In adults, this ectopic induction manifests as a 'Multivulva' (Muv) phenotype, which is characterized by large protrusions formed of ectopic vulval tissue flanking the normal vulva.

The fates of individual VPCs can be assessed during larval development using the primary fate marker *arIs222[lag-2p::2×NLS-tagRFP]*, which is normally expressed only in P6.p and its descendants upon activation of ERK by the EGF-like inductive signal (Fig. 3A). Expression of this marker was unaffected in *gsk-3(0)* mutants (Fig. 3B). In *cdk-2(0)* mutants, a small but significant percentage of larvae displayed ectopic primary fate marker expression, although most VPCs did not (Fig. 3C). The lack of an overt effect on vulval cell fates by single mutants has been observed for many other negative regulators of EGFR-Ras-ERK activity, including *sel-10*, because multiple mechanisms operate redundantly (de la Cova and Greenwald, 2012; Hajnal et al., 1997; Hopper et al., 2000; Jongeward et al., 1995; Yoo et al., 2004).

LIN-45(V627E) is equivalent to human BRAF(V600E), which has constitutive kinase activity and is the product of the most common mutation of human *BRAF* in melanomas (Lavoie and Therrien, 2015). Using a single-copy insertion transgene (see Materials and Methods), we assessed the effect of LIN-45(V627E) expression on the fates of individual VPCs, based on the presence and pattern of ectopic primary fate marker expression. If expression is spaced in alternating VPCs, then the level of ERK activity is not high enough to overcome the opposing effects of LIN-12/Notch (Berset et al., 2001; Underwood et al., 2017; Yoo et al., 2004). When P5.p and/or P7.p adopt the primary fate despite being adjacent to P6.p, ERK signaling is high enough to prevail. Larvae expressing LIN-45(V627E) displayed ectopic primary fate in P3.p, P4.p or P8.p in 31% of animals (Fig. 3D). Notably, ectopic primary fate was never seen in P5.p or P7.p, nor in two adjacent VPCs, as expected for a moderate level of ERK activation. Larvae expressing LIN-45(V627E) in *gsk-3(0)* or *cdk-2(0)* mutants not only displayed significantly higher frequencies of ectopic primary fate marker expression (Fig. 3E,F), but also expressed this marker in adjacent VPCs (Fig. 3E,F) and occasionally even in P5.p or P7.p, consistent with high levels of Raf-MEK-ERK signaling. Thus, both *gsk-3* and *cdk-2* appear to act as negative regulators of Raf-MEK-ERK signaling and LIN-45 stability, consistent with a role in promoting LIN-45 degradation.

In adults, the penetrance of the Muv phenotype caused by expressing LIN-45(V627E) in VPCs was low (Fig. 3G,H). Loss of *sel-10* increases the penetrance of LIN-45(V627E), causing a highly penetrant Muv phenotype (de la Cova and Greenwald, 2012). Similarly, loss of *gsk-3*, *cdk-2* or *cye-1* increased the penetrance and expressivity of the Muv phenotype of LIN-45(V627E)-expressing adults (Fig. 3G,H), consistent with a role in a negative feedback mechanism.

Because the ectopic primary fate and Muv phenotypes arise from ERK activation in VPCs other than P6.p, these results indicate that GSK-3- and CDK-2-mediated negative feedback can operate in other VPCs. As we have suggested previously for *sel-10* (de la Cova and Greenwald, 2012), opposition to Ras pathway activation may normally help set a high threshold to ensure that only P6.p adopts the primary fate.

An *in vivo* biosensor for ERK activity reveals differences in the roles of GSK-3 and CDK-2 in regulating ERK activity

We assessed the effect of *gsk-3(0)* and *cdk-2(0)* on the level of MPK-1/ERK activity using ERK-nKTR-mClover (ERK-nKTR), a genetically encoded *in vivo* biosensor, as a readout. ERK-nKTR

Development (2020) 147, dev195941. doi:10.1242/dev.195941

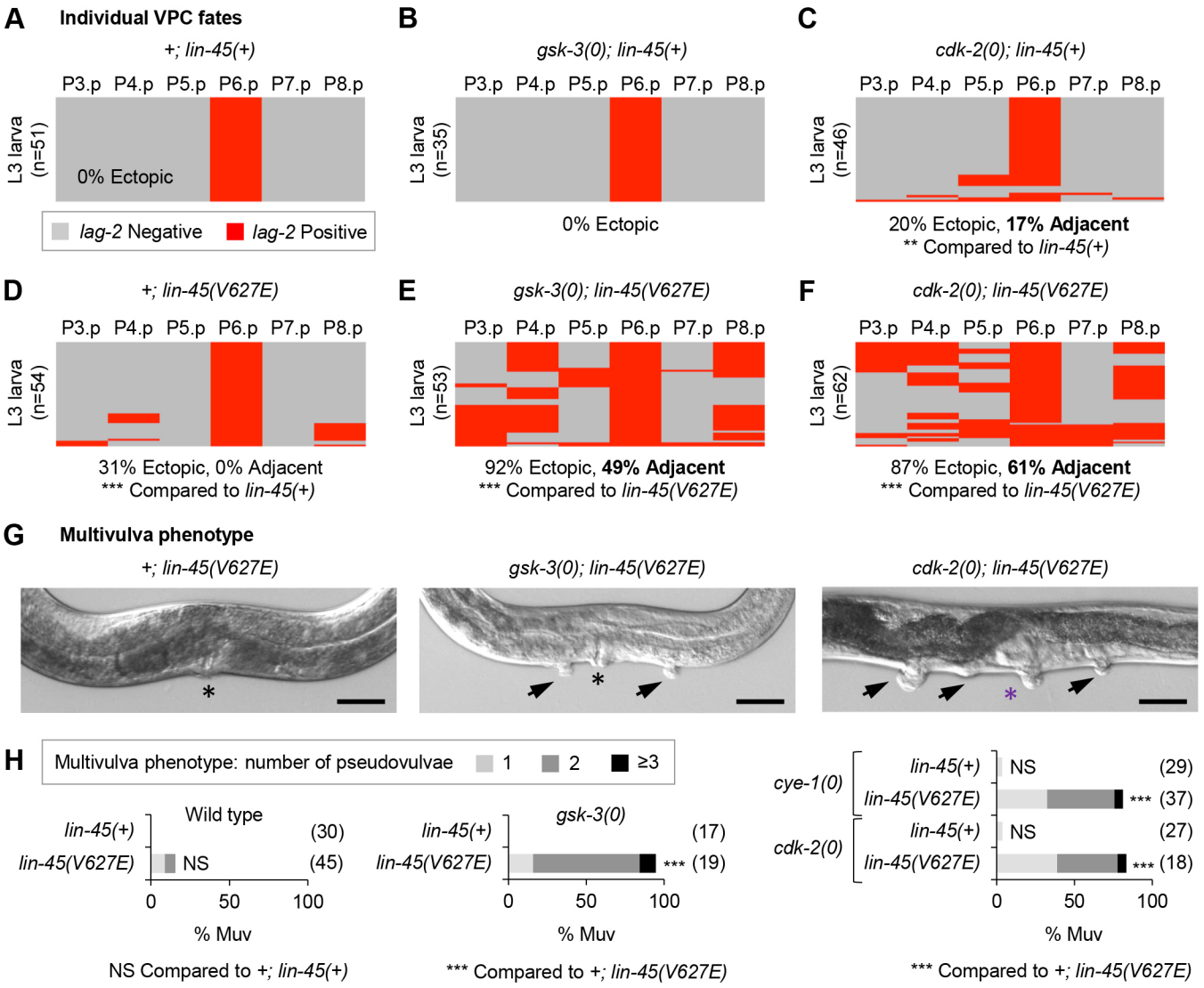

Fig. 3. Loss of either GSK-3 or CDK-2/cyclin E enhances LIN-45(V627E)-driven phenotypes. (A-H) VPC fates and vulva phenotypes of wild type, or the null mutants *gsk-3(0)*, *cye-1(0)* or *cdk-2(0)*. (A-F) Individual VPC fates, assessed using the primary fate reporter *arIs222[lag-2p::2×NLS-tagRFP]*. Shown are: (A) Wild type +; *lin-45(+)*, (B) *gsk-3(0); lin-45(+)* and (C) *cdk-2(0); lin-45(+)*. Genotypes carrying *arTi11* [*lin-31p::lin-45(V627E)*] express the hyperactive LIN-45(V627E) and are: (D) +; *lin-45(V627E)*, (E) *gsk-3(0); lin-45(V627E)* and (F) *cdk-2(0); lin-45(V627E)*. In each panel, rows represent a scored larva, and columns represent the indicated VPCs. Red, *lag-2* is expressed; gray, *lag-2* is not expressed. The number of larvae scored (*n*) and percentage displaying any ectopic *lag-2* expression (% Ectopic) or expression in adjacent VPCs (% Adjacent) is indicated. A two-tailed Fisher's exact test was performed to compare the number of larvae with any ectopic primary fate, and the relevant comparison is indicated below each panel. ***P<0.0001; **P<0.001. (G) Adult hermaphrodites that express LIN-45(V627E) in wild type (left), *gsk-3(0)* (center), or *cdk-2(0)* mutants (right). The location of the normal vulva is indicated by an asterisk; ectopic pseudovulvae are indicated by arrowheads. *cdk-2(0)* mutants have an abnormally everted vulva (see Materials and Methods), indicated by a purple asterisk. Scale bar: 50 µm. (H) Adults were scored for number of pseudovulvae (see Materials and Methods). The percentage of adults displaying the Muv phenotype is shown, with the number scored (*n*) in parentheses. Left, wild-type *lin-45(+)* or those expressing *lin-45(V627E)*. Center, the *gsk-3(0)* mutants with *lin-45(+)* or *lin-45(V627E)*. Right, the *cye-1(0)* and *cdk-2(0)* mutants with *lin-45(+)* or *lin-45(V627E)*. A two-tailed Fisher's exact test was performed to compare the number of adults with any pseudovulvae. The relevant comparison is indicated below each graph. ***P<0.0001; NS, not significant.

allows for quantitation of the degree of MPK-1 activation based on the nucleocytoplasmic localization of a fluorescent protein, mClover, fused to a module that is phosphorylated by MPK-1. When the module is unphosphorylated, mClover is enriched in the nucleus, whereas when the module is phosphorylated, mClover is exported and excluded from the nucleus (de la Cova et al., 2017; Regot et al., 2014). The ERK-nKTR sensor is expressed as a bicistronic transcript with mCherry-histone H2B from a single-copy insertion transgene, ensuring equivalent expression of mClover and mCherry (see Materials and Methods). The degree of MPK-1 activity may be quantified by determining the mCherry:mClover ratio of fluorescence intensity per nucleus (see Materials and Methods; de la Cova et al., 2017).

Because LIN-45 degradation occurs in early L3 (de la Cova and Greenwald, 2012), we examined ERK-nKTR at that time, before VPC division (see Materials and Methods). In wild-type L3 VPCs, ERK-nKTR was excluded from nuclei of P6.p and enriched in the nuclei of P4.p, P5.p, P7.p and P8.p, and quantification revealed that MPK-1 activity was significantly higher in P6.p than in other VPCs (Fig. 4A). Compared with wild-type larvae, LIN-45(V627E) larvae displayed significantly reduced nuclear ERK-nKTR in P4.p, P5.p, P7.p and P8.p, indicating that MPK-1 activity was increased in these cells (Fig. 4B).

Development (2020) 147, dev195941. doi:10.1242/dev.195941

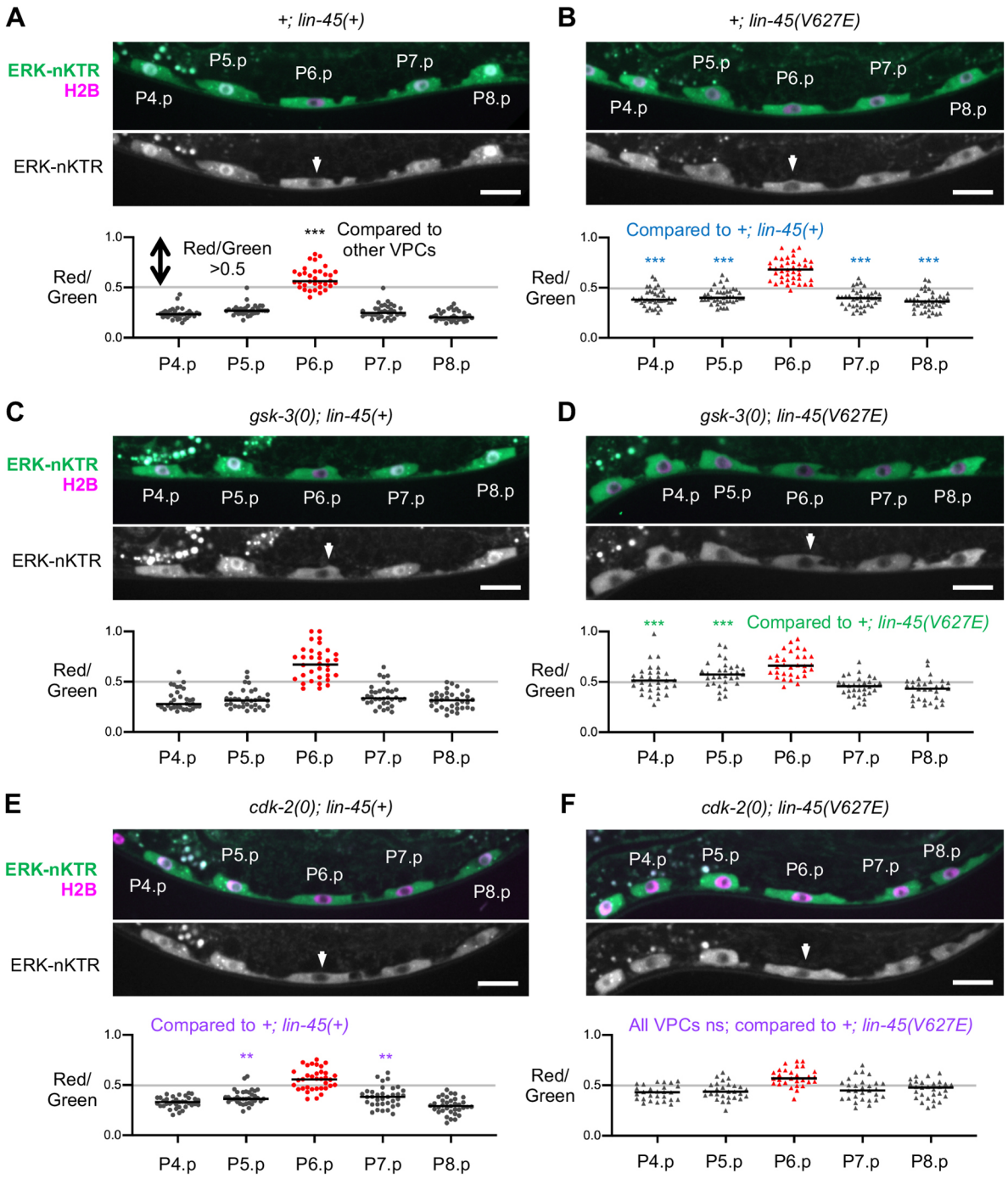

Fig. 4. GSK-3 restrains activation of the downstream kinase ERK by LIN-45(V627E). (A-F) The biosensor *arTi87[ERK-nKTR-mClover::T2A::mCherry-H2B]* was used to quantify ERK activation in VPCs. Throughout, ERK-nKTR-mClover (ERK-nKTR) is shown in green and mCherry-H2B (H2B) is shown in magenta in representative images of L3 stage larvae. ERK-nKTR is also shown separately in grayscale, with P6.p indicated (arrows). In all graphs, ERK activity is quantified as the 'Red/Green' ratio (see Materials and Methods). Each cell analyzed is shown as one data point; those from P6.p are highlighted in red. Median Red/Green ratios are indicated by horizontal black bars. In wild-type larvae, more than 95% of P6.p cells displayed a Red/Green ratio ≥0.5, depicted by a gray gridline on each panel. (A,B) Expression of LIN-45(V627E) increases ERK activity. (A) Top, ERK-nKTR in a *lin-45(+)* larva; bottom, ERK activity (*n*=34). (B) Top, ERK-nKTR in a *lin-45(V627E)* larva; bottom, ERK activity (*n*=40). (C,D) Loss of *gsk-3* increases ERK activation by LIN-45(V627E). (C) Top, ERK-nKTR in a *gsk-3(0)* mutant; bottom, ERK activity (*n*=34). (D) Top, ERK-nKTR in a *gsk-3; lin-45(V627E)* larva; bottom, ERK activity (*n*=32). (E,F) Loss of *cdk-2* increases ERK activity in the *lin-45(+)* background, but not in LIN-45(V627E)-expressing larvae. (E) Top, ERK-nKTR in a *cdk-2(0)* mutant; bottom, ERK activity (*n*=35). (F) Top, ERK-nKTR in a *cdk-2; lin-45(V627E)* larva; bottom, ERK activity (*n*=29). To assess significance, a one-way ANOVA was performed, followed by multiple comparisons and *P*-value correction using the Bonferroni method. For each different genotype, the relevant comparison is indicated on the corresponding graph. ***P<0.0001; **P<0.01; ns, not significant. Scale bars: 10 µm.

We next analyzed ERK-nKTR in *gsk-3(0)* mutants. In a *lin-45(+)* background, *gsk-3(0)* had no obvious effect on ERK-nKTR localization, and MPK-1 activity remained restricted to P6.p (Fig. 4C). When LIN-45(V627E) was expressed in VPCs, quantification revealed that *gsk-3(0)*; *lin-45(V627E)* had increased MPK-1 activity in anterior VPCs (P4.p and P5.p) but not posterior

Development (2020) 147, dev195941. doi:10.1242/dev.195941

VPCs (P7.p and P8.p) compared with the activity in *gsk-3(+); lin-45(V627E)* (Fig. 4D). This anterior-posterior difference may be related to the proximity of posterior VPCs to a strong posterior Wnt signaling source (Sawa and Korswagen, 2013).

By contrast, *cdk-2(0)* affected MPK-1 activity even in a *lin-45(+)* background: in *cdk-2(0)* mutants, ERK-nKTR was less nuclear enriched, and quantification indicated that MPK-1 activity in P5.p and P7.p was significantly increased compared with that in the *cdk-2(+)* background (Fig. 4E), suggesting a role for CDK-2 in fine-tuning the pattern of MPK-1 activation by restricting it to P6.p. However, in *cdk-2(0); lin-45(V627E)* mutants, the level of MPK-1 activity was not increased compared with that of *cdk-2(+); lin-45(V627E)* larvae, despite the high penetrance of ectopic primary fate observed in this genotype (Fig. 4F). This result suggests that the Muv and ectopic primary fate phenotypes observed may be caused by an alternative mechanism and not further elevated MPK-1 activity. We consider the role of *cdk-2* further below.

Constitutive MPK-1 activity causes LIN-45 degradation, but does not bypass the requirement for GSK-3 and CDK-2 activity

MPK-1 is necessary for degradation of LIN-45 in P6.p (de la Cova and Greenwald, 2012). To test whether activating MPK-1 is sufficient to promote degradation, we used the transgene *gaIs37*, referred to hereafter as ERK(act), which constitutively activates MPK-1 in all VPCs and causes a highly penetrant Muv phenotype (Eisenmann et al., 1998; Lackner and Kim, 1998). ERK(act) produced ectopic expression of the primary fate marker *lag-2p::2×NLS-tagRFP* at high frequency (Fig. 5A; Fig. S3) and caused YFP-LIN-45 protein levels to be very low, or not visible, in VPCs (Fig. 5A,B). Thus, ERK(act) is sufficient to induce LIN-45 degradation in all VPCs. We found that in L3 stage *gsk-3(0)* mutants carrying YFP-LIN-45 and ERK(act), YFP-LIN-45 was frequently stable in P5.p, P6.p and P7.p (Fig. 5B), indicating that strong activation of MPK-1 does not bypass the need for *gsk-3* activity in LIN-45 degradation.

Because animals containing ERK(act) and *cdk-2(0)* grew poorly due to apparent pleiotropic effects, we reduced *cdk-2* activity by an alternative approach that does not compromise viability or fertility. Expression of the CDK-interacting protein/kinase inhibitory protein (Cip/Kip) CKI-1 using the *egl-17* promoter (*egl-17p*) causes CDK inactivation and results in incompletely penetrant cell cycle arrest (Hong et al., 1998). The *egl-17* promoter is activated in P6.p in response to MPK-1 activation (Burdine et al., 1998). Using a *egl-17p::cki-1* transgene (see Materials and Methods) combined with YFP-LIN-45, we identified individual larvae in which P6.p was arrested while P5.p and P7.p had divided (Fig. 5C), and other individuals in which P6.p was not arrested. We found that LIN-45 degradation was abrogated when P6.p was arrested (Fig. 5C,D) but usually did occur when P6.p was not arrested. Furthermore, when we combined the *egl-17p::cki-1* and ERK(act) transgenes, VPCs other than P6.p also displayed incompletely penetrant cell cycle arrest (Fig. 5E), because ERK(act) drives *egl-17p::cki-1* expression in all VPCs. In VPCs that were arrested, YFP-LIN-45 degradation was prevented (Fig. 5F). Thus, as for *gsk-3*, high MPK-1 activity does not bypass the requirement for *cdk-2* in LIN-45 degradation.

CDK-2 activity specifies the temporal pattern of LIN-45 protein degradation

In the L2 stage, VPCs remain in a G0/G1-like phase as a result of CDK inhibition by CKI-1; in the L3 stage, diminished expression of CKI-1 allows CDK activation and progression through the cell cycle to mitosis (Fig. 6A) (Kipreos and van den Heuvel, 2019). We previously showed that MPK-1 is activated in P6.p early in the L2 stage (de la Cova et al., 2017), and that LIN-45-YFP is degraded in the L3 stage (de la Cova and Greenwald, 2012). We therefore hypothesized that the timing of LIN-45 degradation might be controlled by the onset of CDK-2 activity.

We first examined YFP-LIN-45 protein expression in larvae staged by milestones of somatic gonad development (see Materials and Methods), and found that all VPCs in wild-type mid-L2 stage larvae express YFP-LIN-45 (Fig. 6B), a time point when MPK-1 is active in P6.p (de la Cova et al., 2017). This result suggests that LIN-45 protein is protected from degradation in the L2 stage, consistent with the hypothesis that CDK-2 activity provides a temporal gate for LIN-45 degradation. We then tested an alternative hypothesis, that LIN-45 is stable in the L2 stage due to insufficient MPK-1 activation, by examining YFP-LIN-45 in L2 stage larvae carrying ERK(act). YFP-LIN-45 was present in all VPCs (Fig. 6F,G), indicating that strong MPK-1 activation is not sufficient to overcome the L2 block to LIN-45 degradation.

If CDK-2 provides a temporal gate, we would expect that precocious CDK activation would cause precocious LIN-45 degradation. In *C. elegans*, the phosphatase CDC-14 is required to maintain cell cycle quiescence of blast cells. In *cdc-14* null mutants, referred to here as *cdc-14(0)*, VPCs fail to express CKI-1 and display incompletely penetrant premature cell division during the L2 stage (Saito et al., 2004). Precocious cell cycle progression of VPCs in the L2 stage does not cause precocious expression of fate markers or overt abnormalities of adult vulval morphology, suggesting that the only consequence of removing *cdc-14* activity is CDK activation (Karp and Greenwald, 2013; Saito et al., 2004). Indeed, when *cdc-14(0)* VPCs divide precociously in the L2 stage, their daughter cells also behave like uncommitted VPCs (Clayton et al., 2008; Saito et al., 2004).

We took advantage of the incomplete penetrance of the *cdc-14(0)* mutant phenotype. When P6.p did not divide, we inferred that CDK activity had remained low; when P6.p did divide, we inferred that CDK activity had been elevated. In *cdc-14(0)* mutants, when P6.p had not divided prematurely, it displayed YFP-LIN-45, as in wild type (Fig. 6B,D). In contrast, when P6.p had divided prematurely, YFP-LIN-45 was degraded in one or both P6.p VPC-like daughters at a significant frequency (Fig. 6C, E). These results suggest that, normally, the onset of CDK-2 activation in the L3 stage is the temporal signal that triggers MPK-1-dependent LIN-45 degradation. In cases where P6.p divided but only one of its daughters displayed YFP-LIN-45 degradation, it may be that the different outcomes in each VPC-like daughter reflect the incomplete penetrance of the *cdc-14(0)* mutant phenotype, or that there is an additional regulatory mechanism in the L2 stage that also opposes degradation.

DISCUSSION

We previously showed that MPK-1 activity is necessary for LIN-45 degradation in P6.p as part of a negative-feedback loop in response to the EGF-like inductive signal (de la Cova and Greenwald, 2012). This negative feedback requires SEL-10, the substrate recognition component of the multiprotein SCF E3 ubiquitin ligase, and a sequence in LIN-45 called the CPD, which would be expected to act as a high-affinity binding site for SEL-10. Here, we identified sequence requirements other than the CPD for LIN-45 degradation in P6.p, including potential phosphorylation sites, showed that ectopic activation of MPK-1 is capable of promoting LIN-45 degradation in all VPCs and identified two additional kinases, GSK-3 and CDK-2,

Development (2020) 147, dev195941. doi:10.1242/dev.195941

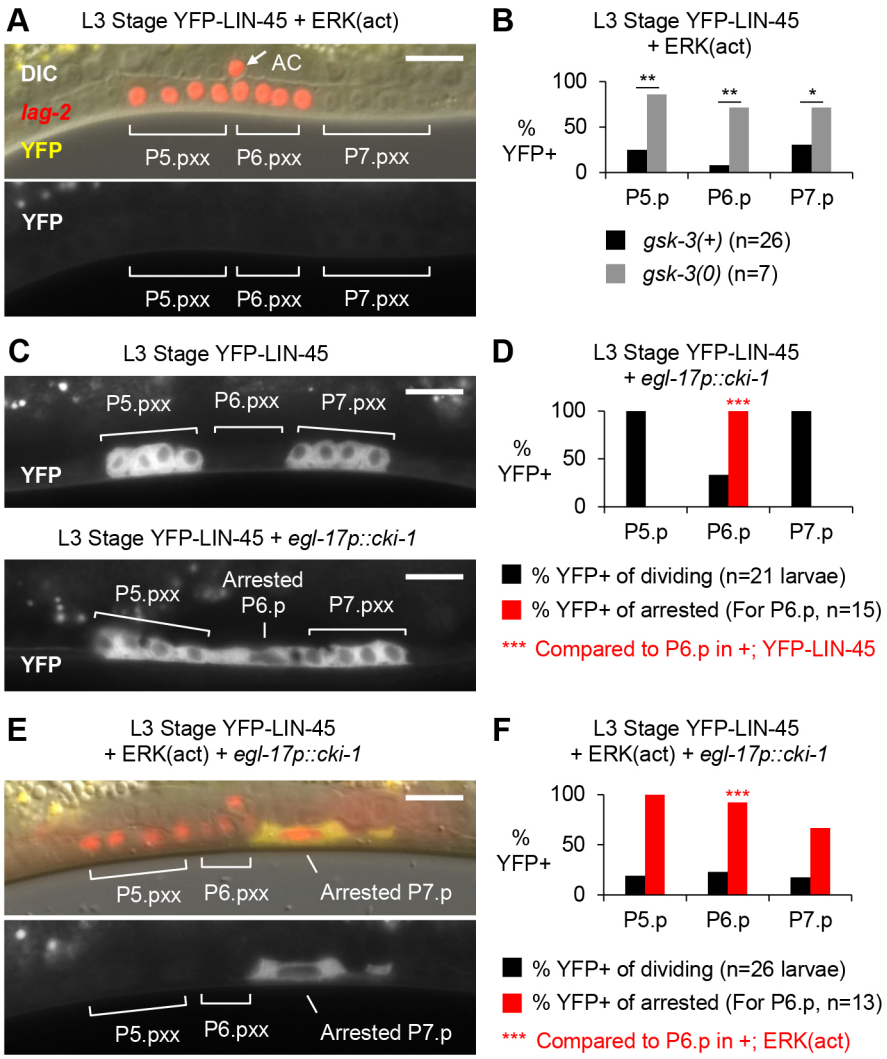

Fig. 5. Constitutive ERK activity causes LIN-45 degradation, but does not bypass the requirement for GSK-3 and CDK-2 activity. (A-F) L3 stage larvae in which at least some VPCs had divided were scored so that cell cycle arrest caused by the *arEx2192[egl-17p::cki-1]* transgene could be assessed (see Materials and Methods). The four granddaughters of a VPC are collectively termed Pn.pxx. (A) Full-length YFP-LIN-45 (yellow) and *arIs222[lag-2p::2×NLS-tagRFP]* (red) in the presence of highly activated MPK-1/ERK, termed ERK(act). Separate panels show the merged fluorescence and DIC image (top) and the YFP-LIN-45 signal in grayscale (bottom). (B) Percentage of VPCs positive for YFP-LIN-45 in the presence of ERK(act), either in *gsk-3(+)* (black) or *gsk-3(0)* (gray) background. *n* indicates the number of larvae scored. For each VPC, a two-tailed Fisher's exact test was performed to compare the number of YFP-positive cells in *gsk-3(+)* and *gsk-3(0)*. (C) Full-length YFP-LIN-45 in L3 stage larvae. Top, normal pattern of YFP-LIN-45 accumulation in a wild-type background. Bottom, at incomplete penetrance in larvae carrying *arEx2192[egl-17p::cki-1]*, P6.p remained undivided, while P5.p and P7.p had divided. (D) Percentage of VPCs positive for YFP-LIN-45 in larvae that express CKI-1 from *arEx2192[egl-17p::cki-1]*. Data is shown for animals in which P5.p and P7.p had divided and P6.p was either arrested (% YFP+ of arrested, red) or had divided (% YFP+ of dividing, black). *n* indicates the number of larvae scored. A two-tailed Fisher's exact test was performed to compare the number of YFP-positive cells in the arrested P6.p cells of *egl-17p::cki-1* (For P6.p, *n*=15) and in P6.p cells of wild type (*n*=34). (E) Full-length YFP-LIN-45 (yellow) and *arIs222[lag-2p::2×NLS-tagRFP]* reporter (red) in the presence of both ERK(act) and *arEx2192[egl-17p::cki-1]*. In these larvae, VPCs other than P6.p failed to divide, presumably because activated ERK induced ectopic expression of *egl-17p::cki-1*. In this example, P5.p and P6.p had generated granddaughters, but P7.p remained undivided. (For frequencies of arrest, see F). Top, merged fluorescence and DIC image; bottom, YFP-LIN-45 signal in grayscale. (F) Percentage of VPCs positive for YFP-LIN-45 in larvae that express both ERK(act) and CKI-1. *n* indicates the number of larvae scored. Data are shown for animals in which some VPCs had divided, and the VPCs were scored as either arrested (% YFP+ of arrested, red) or had divided (% YFP+ of dividing, black). Arrest occurred with incomplete penetrance in P5.p (1/26), P6.p (13/26) and P7.p (3/26). A two-tailed Fisher's exact test was performed to compare the number of YFP-positive arrested P6.p cells of *egl-17p::cki-1*; ERK(act) (for P6.p, *n*=13) with the number of YFP-positive P6.p cells of +; ERK(act) (*n*=26). ****P*<0.0001; ***P* <0.001; **P*-value <0.01. Scale bars: 10 µm.

as essential for the negative-feedback mechanism in P6.p and threshold-setting in other VPCs. In this Discussion, we (1) propose a model for how the combined activities of MPK-1, GSK-3 and CDK-2 are required for LIN-45 degradation, and how MPK-1 and CDK-2 provide spatial and temporal information; (2) consider potential molecular mechanisms by which these kinases operate based on studies of other SEL-10/FBXW7 substrates; and (3) consider to what extent the SEL-10/FBXW7- and MPK-1/ERK-mediated regulation of LIN-45 is conserved in the case of human BRAF regulation.

Kinase control of negative feedback in the EGFR-Ras-Raf-ERK cascade in VPC fate patterning

During vulval induction, negative feedback acting on LIN-45 in VPCs is spatially restricted to P6.p and temporally restricted to the

Development (2020) 147, dev195941. doi:10.1242/dev.195941

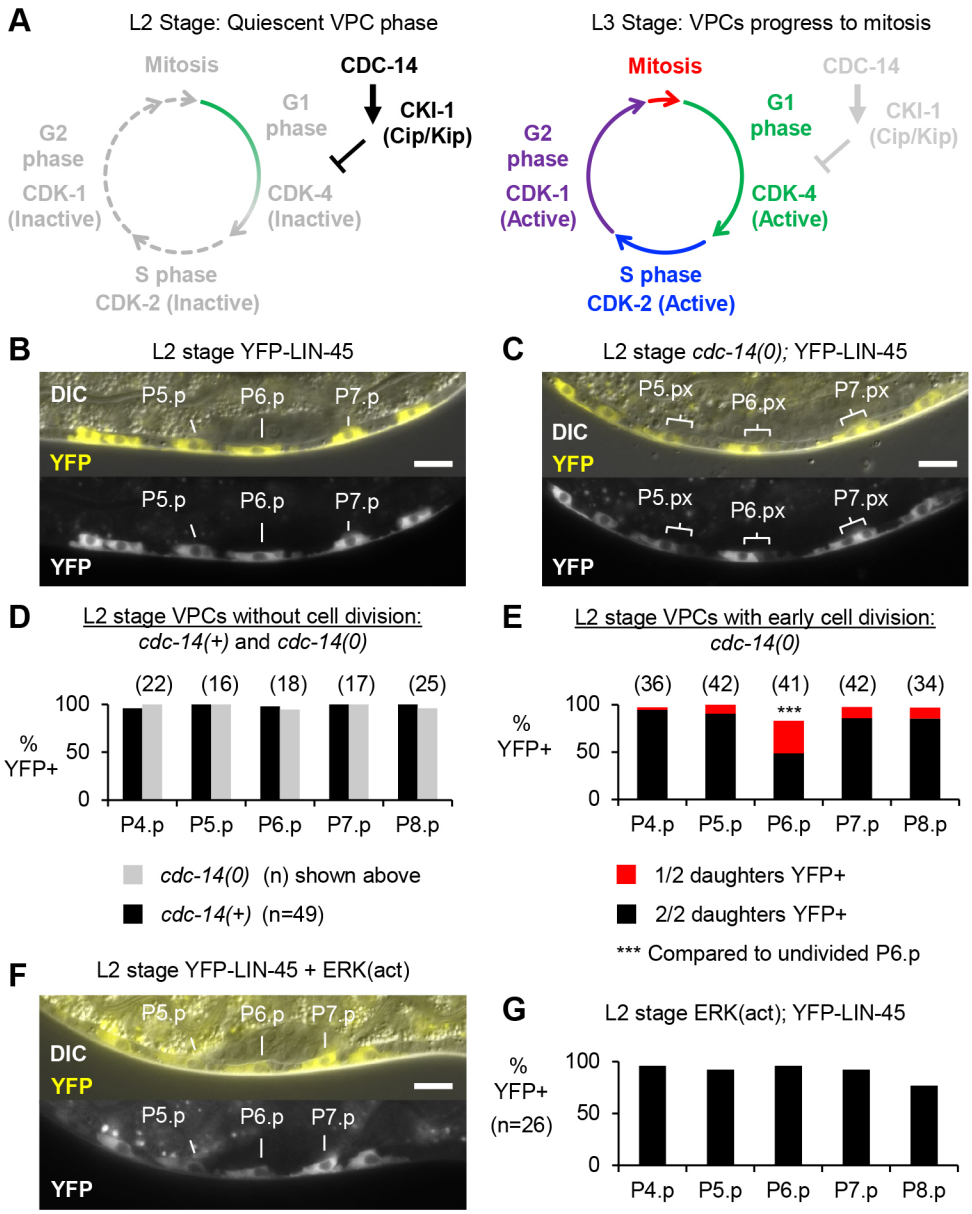

Fig. 6. CDK-2 activity specifies the temporal pattern of LIN-45 protein degradation. (A) In the L2 stage, VPCs remain in a G0/G1-like phase because of high CDC-14 activity and CKI-1 expression. In the L3 stage, expression of CKI-1 is low, allowing CDK activation and progression through the cell cycle. (B) Full-length YFP-LIN-45 in a wild-type larva during the mid-L2 stage. L2 stage larvae were staged using milestones in somatic gonad development (see Materials and Methods). Separate panels show DIC (gray) and YFP-LIN-45 (yellow) merged, and YFP-LIN-45 in grayscale. (C) Full-length YFP-LIN-45 in a *cdc-14(0)* null mutant in the mid-L2 stage. Early cell division of VPCs in the *cdc-14* mutant is incompletely penetrant; in the larva shown, P5.p, P6.p and P7.p have divided precociously in the mid-L2 stage. Separate panels show DIC (gray) and YFP-LIN-45 (yellow) merged, and YFP-LIN-45 in grayscale. (D) Percentage of mid- and late-L2 stage VPCs positive for YFP-LIN-45 when the VPCs were undivided. For the *cdc-14(0)* genotype, sample sizes are reported per VPC (above the graph). (E) Percentage of mid- and late-L2 stage daughters of VPCs positive for YFP-LIN-45 after precocious division in the *cdc-14(0)* mutant. In some cases, both daughters continued to express YFP-LIN-45 (2/2 daughters positive, black); in other cases, either one of two daughters was positive (1/2 daughters positive, red), or neither were positive. For *cdc-14(0)*, sample sizes are reported per VPC (above the graph). A two-tailed Fisher's exact test was performed to compare the number of divided P6.p cells where both daughters had stable YFP-LIN-45 (2/2 daughters YFP+) in *cdc-14(0)* with the number of undivided P6.p cells, where LIN-45 is essentially always stable (YFP+) in either *cdc-14(+)* or *cdc-14(0)* mutants. ***P<0.0001. (F) Full-length YFP-LIN-45 in a representative mid-L2 stage larva in the presence of ERK(act). Separate panels show DIC (gray) and YFP-LIN-45 (yellow) merged, and YFP-LIN-45 in grayscale. (G) Percentage of mid- and late-L2 stage VPCs positive for YFP-LIN-45 in the presence of ERK(act). *n* indicates the number of larvae scored. Scale bars: 10 µm.

L3 stage. We propose a model for how the activities of three kinases, MPK-1, GSK-3 and CDK-2, combine to provide this information (Fig. 7A,B).

MPK-1 was an obvious candidate for providing spatial information because it is more highly activated in P6.p compared with other VPCs due to proximity to the AC. Indeed, engineering high MPK-1 activity in all VPCs is sufficient to cause LIN-45 protein degradation in all VPCs in the L3 stage, supporting this role in defining the spatial pattern in VPCs. However, activated MPK-1 does not bypass the requirement for GSK-3 and CDK-2, suggesting that it functions upstream of or in parallel to them, and does not cause premature degradation in the

Development (2020) 147, dev195941. doi:10.1242/dev.195941

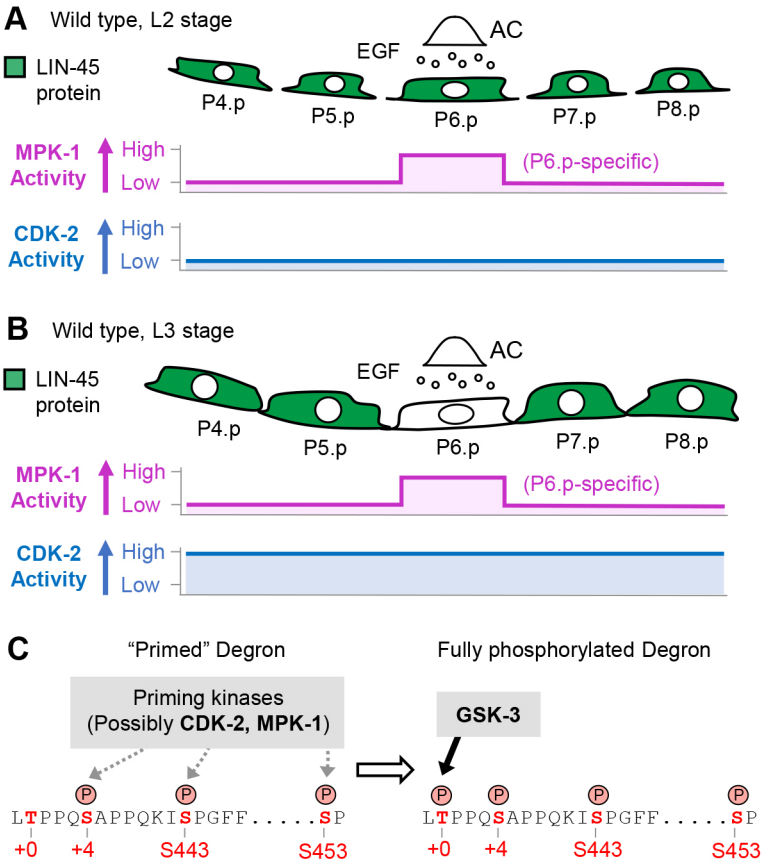

Fig. 7. Spatial and temporal patterning of LIN-45 degradation in wild-type larvae results from combined kinase activities. (A) During the L2 stage, MPK-1 activity (magenta) is high in P6.p and low in other VPCs, whereas CDK-2 activity (blue) is low in all VPCs. LIN-45 protein (green) is not degraded and accumulates in all VPCs. (B) During the early L3 stage, MPK-1 activity remains high in P6.p, and CDK-2 activity becomes high in all VPCs. At this stage, the kinase activities of MPK-1 and CDK-2 coincide in P6.p, and LIN-45 protein is degraded specifically in this cell. (C) Possible roles of kinases in regulating LIN-45 degron phosphorylation. The LIN-45 degron sequence from L431 to P454 is shown; Thr and Ser residues required for degradation are highlighted in red. We propose that MPK-1 and CDK-2 act as priming kinases that are responsible for phosphorylation of the +4 Ser of the CPD, and the S443 and S453 sites defined in this study. Once primed, then GSK-3 is capable of phosphorylating the +0 Thr. A fully phosphorylated degron results in binding by SEL-10 and degradation of LIN-45.

L2 stage, indicating that there is a temporal gate to LIN-45 degradation.

Our analysis indicates that CDK-2, with its associated cyclin, cyclin E, provides a temporal cue that restricts LIN-45 degradation to the L3 stage, even though MPK-1 is active in P6.p in the L2 stage (de la Cova et al., 2017). In the *cdc-14* mutant, when CDKs are inappropriately activated during the L2 stage (Saito et al., 2004), we observed precocious LIN-45 degradation in P6.p. Thus, in wild-type VPCs, LIN-45 protein is degraded where MPK-1 and CDK-2 kinase activities coincide: in P6.p during the L3 stage.

Although GSK-3 does not appear to provide spatial or temporal information per se, its potential role is suggested by mammalian GSK3B. As described more fully in the next section, GSK3B phosphorylates the CPDs of many different FBXW7 substrates on the +0 Thr CPD residue of a previously phosphorylated 'primed' degron, resulting in a fully phosphorylated CPD that allows for recognition by FBXW7. Thus, in our model, we propose a specific mechanistic role for GSK-3 as a +0 Thr kinase, with MPK-1 and CDK-2 as potential priming kinases for initiation of LIN-45 degradation (Fig. 7C).

Lessons from GSK3B, CDK2 and ERK regulation of other FBXW7 substrates for regulation of LIN-45/Raf

The three kinases we identified as regulating the spatial and temporal stability of LIN-45 have also been implicated in the regulation of the stability of other FBXW7 substrates. In humans, the best-studied substrates of FBXW7 are oncoproteins that regulate the cell cycle and growth of mammalian cells, including MYC, JUN, cyclin E and NOTCH1 proteins (reviewed by Yumimoto and Nakayama, 2020). Some of these substrates are also known to be modulated by GSK3B, CDK2 or ERK. Each of these kinases has substrate docking or phospho-acceptor site preferences that we review below; however, the degeneracy found in actual substrates makes it difficult to exclude direct phosphorylation using prediction alone. Nevertheless, the roles of GSK3B, CDK2 and ERK in regulating other FBXW7 substrates provide lessons on degradation of LIN-45.

GSK3B regulates FBXW7 binding and degradation of human MYC, JUN, cyclin E and NOTCH1, in each case by phosphorylating the +0 Thr of the substrate CPD (Espinosa et al., 2003; Wei et al., 2005; Welcker et al., 2004, 2003; Yada et al., 2004). As is true for a large number of GSK3B substrates, these sites conform to the consensus [S/T]-x-x-x-p[S/T], where a prior 'priming' phosphorylation present at the +4 position is recognized by a phosphate-binding pocket of GSK3B and greatly increases affinity (Frame et al., 2001). We propose that GSK-3 promotes LIN-45 degradation through phosphorylation at the +0 Thr residue, providing potential roles for MPK-1 and/or CDK-2 in priming (Fig. 7C). Intriguingly, in human cells, ERK promotes priming phosphorylation at the +4 Ser of the MYC CPD, but it is unclear whether this phosphorylation is direct (Sears et al., 2000). Indeed, other kinases, including CDK2, phosphorylate the MYC CPD +4 Ser *in vitro*, and contribute to MYC phosphorylation and degradation *in vivo* (Hydbring et al., 2010). Some FBXW7 substrates, such as SREBP, contain additional priming sites C-terminal to the +4 Ser (Bengoechea-Alonso and Ericsson, 2009). The two proline-directed sites we identified downstream of the LIN-45 CPD may therefore serve a priming function for one or both phosphorylations of the CPD.

Development (2020) 147, dev195941. doi:10.1242/dev.195941

As a proline-directed kinase, CDK2 strongly favors [S/T]-P phospho-acceptor sites (Chi et al., 2008), often containing a basic residue at positions C-terminal to the phospho-acceptor (Brown et al., 1999; Hodeify et al., 2011; Lees et al., 1992). However, there are many exceptions: for example, in human cells, CDK2 phosphorylates the +4 Ser residue of a high-affinity CPD of cyclin E that lacks a proline (Welcker et al., 2003). Thus, CDK-2 may be capable of phosphorylating several sites of the *C. elegans* LIN-45, including the +4 Ser, which does not have an adjacent proline, and/or the two S-P sites we identified in this work.

Many well-characterized MPK-1/ERK substrates in mammals and *C. elegans* contain docking sites with a 'D domain' motif (also known as a KIM or DEJL sequence) characterized by the consensus sequence [K/R]-x(0-5)-L-x-L, and/or a 'DEF' motif with the consensus F-x-F-P (Arur et al., 2009; Fantz et al., 2001; Jacobs et al., 1999). Although the LIN-45(430-480) region that is sufficient for P6.p-specific degradation does not contain an obvious docking site, it is formally possible that MPK-1 acts as a priming kinase through a non-canonical site. However, insights into the mechanism underlying the spatial specificity provided by MPK-1 may be gleaned from mammalian studies, where ERK impacts activities of FBXW7, CDK2 and GSK3B by a number of mechanisms. For example, in some human cell contexts, ERK signaling stimulates CDK2 activity, likely by an indirect mechanism mediated by the upstream CDK-activating kinase CDK7 (Chiariello et al., 2000; Lents, 2002). In *C. elegans*, Arur et al. (2009) found that both GSK-3 and CDK-7 proteins are direct substrates of MPK-1, and knockdown of either kinase produces germline phenotypes consistent with a role in negative feedback on MPK-1 signaling. Because activated MPK-1 does not bypass the need for *gsk-3* or *cdk-2*, we propose that GSK-3 and CDK-2 do not act upstream of MPK-1.

Conservation of SEL-10/FBXW7-mediated, Ras-ERK cascade-dependent Raf protein degradation

In mammalian cells, Raf-MEK-ERK cascade activation results in negative feedback via phosphorylation of BRAF, inactivation and degradation (Grbovic et al., 2006; Hernandez et al., 2016; Ritt et al., 2010; Saei et al., 2018), as we have observed for LIN-45/Raf. Indeed, Hernandez et al. (2016) provide strong support for conservation of the MPK-1- and CPD-dependent degradation that we described for *C. elegans* LIN-45, showing that the level and half-life of BRAF depends on ERK activity and that mutation of the +0 Thr or +4 Ser residues of the conserved CPD increases BRAF stability in a mouse embryonic fibroblast cell line.

At least in some cell contexts, this negative feedback involves FBXW7. Saei et al. (2018), using human HEK293 cells, demonstrated that FBXW7 physically interacts with BRAF, and observed a loss of polyubiquitylation of BRAF protein after siRNA-mediated knockdown of *FBXW7*. Although Hernandez et al. (2016) concluded that ERK- and CPD-dependent negative-feedback regulation of BRAF is not mediated by FBXW7, their conclusion was based on the finding that BRAF is still degraded in the presence of a missense mutation in the substrate-binding domain, FBXW7 (R482Q). Because FBXW7 (R482Q) can still bind to BRAF and retains the F-box domain that mediates SCF complex interaction, the depletion experiments of Saei et al. (2018) appear more compelling, and suggest that the negative-feedback loop we have identified in P6.p may operate via SEL-10/FBXW7 in some cell contexts. We therefore propose that our findings of additional kinases that mediate the degradation of LIN-45 in *C. elegans* may also be relevant to such mammalian contexts.

MATERIALS AND METHODS

C. elegans genetics

All *C. elegans* strain names and full genotypes are listed in Table S1. The following mutant alleles were obtained from the National BioResource Project *C. elegans* (NBRP *C. elegans*, https://shigen.nig.ac.jp/c.elegans/). LGI: *cdk-2(tm2244)*; *gsk-3(tm2223)*. The following alleles were obtained from the Caenorhabditis Genetics Center (CGC; https://cgc.umn.edu/). LGII: *cdc-14(he141)* (Saito, et al., 2004). LGIII: the transgene *gaIs37 [Ef1a::dSor, hs::mpk-1]* (Eisenmann, et al., 1998). The allele *cye-1(ar95)* was previously described (Fay and Han, 2000). The RNAi-sensitized mutant *nre-1(hd20) lin-15B(hd126)* displays enhanced RNAi effectiveness in VPCs (Deng et al., 2019; Schmitz et al., 2007). The transgene *arIs222 [lag-2p::2×NLS-tagRFP::unc-54 3′UTR]* was previously described (Sallee and Greenwald, 2015; Underwood et al., 2017). Because homozygous individuals were sterile, animals carrying *gsk-3(tm2223)*, *cdk-2(tm2244)* or *cye-1(ar95)* alleles were maintained as balanced heterozygotes. Homozygous individuals were scored based on lack of a fluorescent GFP-tagged balancer chromosome.

Plasmids and transgenes used for *lin-45* expression in *C. elegans*

Plasmids for *lin-45* reporter transgenes were generated following a method described in de la Cova and Greenwald (2012). Specifically, the YFP-coding sequence was fused in frame with *lin-45* cDNA (Wormbase sequence Y73B6A.5a) to produce a sequence encoding N-terminally tagged YFP-LIN-45 protein. For expression of YFP-LIN-45 in VPCs, cDNAs were cloned into pCC249, an expression vector in a miniMos backbone (Frøkjær-Jensen et al., 2014) that contains a hybrid promoter derived from 5′ and intronic elements of the *lin-31* gene, designated *lin-31p* (Tan et al., 1998), and a 3′ UTR derived from the *unc-54* gene. Other than the specified mutations generated in YFP-LIN-45, all regulatory and surrounding sequences are identical in the plasmids reported. For rescue of *gsk-3* and *cye-1* mutants, *gsk-3* and *cye-1* cDNAs were amplified from the ProQuest *C. elegans* cDNA library (Invitrogen) and cloned into the pCC249 expression vector.

New transgenes generated in this work are described in Table S2. Single-copy miniMos insertion transgenes were generated by germline injection of N2 strain hermaphrodites with 10 ng/µl reporter plasmid and a co-injection mixture of pCFJ601, pCFJ90, pGH8 and pMA122 Frøkjær-Jensen et al. (2014); strains carrying integrated reporters were isolated as described by Frøkjær-Jensen et al. (2014). Extrachromosomal transgenes were generated by germline injection of *pha-1(e2123)* mutant hermaphrodites with a mixture of ScaI-digested reporter plasmid (1 ng/µl), pCW2.1 [ceh-22p::GFP] (1 ng/µl), pBX [pha-1(+)] (1 ng/µl) and digested N2 genomic DNA (50 ng/µl), as described previously (de la Cova and Greenwald, 2012).

C. elegans transgenes used to report or alter VPC gene expression

lin-31p::2×NLS-YFP

The single-copy integrated transgene *arTi88* (this work) contains the *lin-31p* elements described above, and drives expression of 2×NLS-YFP. Expression from *lin-31p* is approximately uniform in L3 stage VPCs (de la Cova and Greenwald, 2012). We scored *arTi88* expression in wild type larvae and in *gsk-3*, *cdk-2* and *cye-1* mutants at the L3 stage and found that *lin-31p*-driven transcription was active in all VPCs of these genotypes (Fig. S4).

lin-31p::YFP-lin-45

The single-copy integrated transgene *arTi94* (this work) uses *lin-31p* to drive expression of a full-length YFP-tagged LIN-45. Protein accumulation of YFP-LIN-45 in L2 and L3 stage VPCs is described in this work and by de la Cova and Greenwald (2012).

lag-2p::2×NLS-tagRFP

The integrated transgene *arIs222* (Sallee and Greenwald, 2015) uses 5′ sequences of the *lag-2* gene to drive expression of *2×NLS-tagRFP*. This reporter is expressed exclusively in P6.p and daughters at the L3 stage. For data reported on YFP-LIN-45 expression, we examined *arIs222* in the same larvae to ensure that *lag-2* was expressed in P6.p, an indicator that Raf-MEK-ERK signal transduction and subsequent primary cell fate induction had occurred.

Development (2020) 147, dev195941. doi:10.1242/dev.195941

lin-45(V627E)

The single-copy integrated transgene *arTi11* (this work) uses the *lin-31p* elements to drive expression of a mutant cDNA, *lin-45(V627E)*, followed by a 3′ UTR derived from the *unc-54* gene.

gsk-3(+)

The single-copy integrated transgene *arTi129* (this work) uses the *lin-31p* elements to drive expression of wild-type *gsk-3* cDNA (Wormbase sequence Y18D10A.5), followed by a 3′ UTR derived from the *unc-54* gene.

cye-1(+)

The single-copy integrated transgene *arTi7* (this work) uses the *lin-31p* elements to drive expression of wild-type *cye-1* cDNA (Wormbase sequence C37A2.4a), followed by a 3′ UTR derived from the *unc-54* gene.

ERK-nKTR

The single-copy integrated transgene *arTi87* (this work) uses the *lin-31p* elements to drive expression of a bi-cistronic *ERK-KTR-mClover-T2A-mCherry-his-11* cDNA, followed by a 3′ UTR derived from the *unc-54* gene. This transcript produces two separate reporter proteins, ERK-KTR-mClover and mCherry-HIS-11, as described previously (de la Cova, et al., 2017).

ERK(Act)

The integrated transgene *gaIs37* was described previously (Eisenmann et al., 1998). The Multivulva phenotype and adult lethality produced by *gaIs37* is most severe at higher temperatures. To avoid lethality, strains carrying *gaIs37* were maintained at 15°C; larvae scored for all experiments were collected and grown at 20°C.

egl-17p::cki-1

Elements derived from sequence 5′ of the *egl-17* gene are capable of driving expression in P6.p during the L3 stage (Burdine et al., 1998). The extrachromosomal transgene *arEx2192* (this work) uses these elements from *egl-17* to drive expression of wild-type *cki-1* cDNA (Wormbase sequence T05A6.1), followed by a 3′ UTR derived from the *unc-54* gene. Like other reported *egl-17p::cki-1* transgenes (Hong et al., 1998; Nusser-Stein et al., 2012), *arEx2192* produces cell cycle arrest at incomplete penetrance. P6.p was scored as arrested if P6.p was undivided while P5.p and P7.p had divided to produce at least two daughters.

Screen of conserved kinases by RNAi treatment in *C. elegans*

RNAi-feeding bacteria strains that target 248 different *C. elegans* protein kinases that have known or predicted orthology with human kinases (Deng et al., 2019; Kim et al., 2018) were used for our RNAi-feeding screen. Each bacteria strain was grown in liquid culture and spread on NGM plates containing IPTG inducer, as previously described (Kamath et al., 2003). The extrachromosomal array *arEx1820* contains *lin-31p*-driven *yfp-lin-45(417-480)*. This array produces very bright expression of the truncated YFP-LIN-45(417-480) protein, making it useful for our visual screen. The *C. elegans* strain GS7213, genotype *pha-1(e2123); nre-1(hd20) lin-15B(hd126); arEx1820[yfp-lin-45(417-480)]*, was treated with a standard bleach/sodium hydroxide protocol to prepare eggs (Stiernagle, 2006). Approximately 200 eggs were placed on each RNAi-feeding plate and grown at 22°C. L3 stage larvae were examined after ∼40 h, a time point when larvae of early, mid and late L3 stage were easily found. Larvae were anesthetized in M9 buffer containing 10 mM levamisole, and the presence of YFP fluorescence in P6.p, daughter cells (P6.px) or granddaughter cells (P6.pxx) was scored qualitatively using 40× magnification and a Zeiss Axio Imager microscope. At least 30 L3 stage larvae were scored for each RNAi treatment.

Assessment of the Multivulva phenotype

To assess the Multivulva phenotype caused by *arTi11[lin-31p::lin-45(V627E)]*, L4 hermaphrodites from uncrowded cultures were picked to fresh plates; adults were examined ∼24 h later using a dissecting microscope and scored for the presence of a normal vulva and the number of pseudovulvae. We note that *cdk-2(0)* mutants display the abnormal vulval eversion (Evl) phenotype previously reported for *cye-1* mutants (Fay and Han, 2000; Seydoux et al., 1993), characterized by a single protrusion at the normal vulval position. To score ectopic vulval induction for *cdk-2(0)* and *cye-1(0)* mutants, the single, central protrusion was treated as the vulva, and supernumerary vulva-like ventral protrusions were scored as pseudovulvae. All *lin-45(+)* and *lin-45(V627E)* animals scored for the Multivulva phenotype were grown at 20°C.

Scoring of fluorescent reporter expression in VPCs

To obtain L2 and L3 stage larvae, egg collections were performed by allowing adult hermaphrodites to lay eggs for 8-16 h. For all experiments with YFP-LIN-45 transgenes and *arIs222[lag-2p::tagRFP],* larvae were grown at 20°C. For scoring and imaging, larvae were anesthetized in M9 buffer containing 10 mM levamisole.

L2 stage larvae were examined ∼24 h after egg collection and more precisely staged based on the location and appearance of presumptive AC/VU cells of the somatic gonad. Specifically, during the early L2, expression of the *arIs222[lag-2p::tagRFP]* transgene is visible in four gonad cells arranged in an anterior-posterior line in the ventral gonad. By mid L2, two of these cells migrate left and right, while the presumptive AC/VU cells remain together at the midline. For data on YFP-LIN-45 protein in the L2 stage, we report larvae scored at mid and late L2.

L3 stage larvae were examined ∼36 h after egg collection. To ensure that the inductive signal was intact in animals of the genotypes scored, we examined larvae for expression of the *arIs222 lag-2p::tagRFP* reporter in P6.p. In addition, larvae were staged based on whether VPCs had divided, a milestone that occurs at the time of cell fate commitment. Unless otherwise specified, for data on YFP-LIN-45 protein in the L3 stage, we report larvae in which P6.p was positive for *lag-2p::tagRFP* and VPCs had divided to produce at least two daughters.

YFP and RFP fluorescence was scored at 40× magnification using a Zeiss Axio Imager microscope, equipped with either a Hamamatsu ORCA-ER or Zeiss Axiocam. For all YFP-LIN-45 reporters, a 500 ms exposure was used to capture the YFP image and qualitatively score VPCs as positive or negative.

Quantification of ERK activity in VPCs

To obtain L3 stage larvae for analysis of the ERK-nKTR biosensor, egg collections were performed by allowing adult hermaphrodites to lay eggs for 2 h. Larvae were grown at 25°C to enhance expression and brightness of the fluorescent ERK-nKTR biosensor, and examined 28-30 h after egg collection. For imaging, larvae were anesthetized in M9 buffer containing 0.5 mM levamisole. *Z*-stacks of mClover and mCherry fluorescence in VPCs were captured simultaneously at the same exposure time and laser power (500 ms, 50% laser), using 63× magnification and a Zeiss spinning-disk dual-camera system. A workflow of ERK-nKTR image quantification has been described previously (de la Cova et al., 2017). Briefly, a ratiometric image called ‘Red/Green’ was produced by dividing mCherry intensity values by mClover intensity values for each pixel. Image segmentation was performed using CellProfiler (Kamentsky et al., 2011). Nuclei were segmented based on the nuclear histone mCherry-H2B signal. For each nucleus, the upper quartile intensity of the ratiometric Red/Green image was obtained, and the mean of the five most equatorial *z* sections is reported as the measurement ‘Red/Green’.

Quantification and statistical analysis

When comparing two genotypes for differences in phenotype penetrance, such as YFP-LIN-45 stability, expression of the *lag-2 arIs222* reporter and the Multivulva phenotype, we used the Fisher’s exact test to calculate a two-tailed *P*-value. When comparing multiple genotypes for differences in mean Red/Green ratio, we performed a one-way ANOVA, followed by pairwise comparisons and *P*-value correction using the Bonferroni method.

Acknowledgements

We thank Katherine Luo, Kennedy Stacy and Elizabeth Johnson for assistance in generating reporter plasmids and transgenic strains, and Daniel Shaye and Catherine O’Keeffe for their valuable comments on this manuscript. Some strains

were provided by the CGC, which is funded by NIH Office of Research Infrastructure Programs (P40 OD010440), and by the NBRP *C. elegans* of the MEXT, Japan.

Competing interests
The authors declare no competing or financial interests.

Author contributions
Conceptualization: C.C.d.l.C., I.G.; Formal analysis: C.C.d.l.C., R.T.; Investigation: C.C.d.l.C., R.T.; Writing - original draft: C.C.d.l.C., I.G.; Writing - review & editing: C.C.d.l.C., R.T., I.G.; Supervision: C.C.d.l.C., I.G.; Project administration: C.C.d.l.C., I.G.; Funding acquisition: I.G.

Funding
This work was supported by a Senior Scholar award from the Ellison Medical Foundation (AG-SS-2951-12 to I.G.); the National Institute of General Medical Sciences (R01GM114140 and R35GM131746 to I.G.); and a research start-up grant from the University of Wisconsin-Milwaukee (to C.C.d.l.C). Deposited in PMC for release after 12 months.

Supplementary information
Supplementary information available online at
https://dev.biologists.org/lookup/doi/10.1242/dev.195941.supplemental

References
Ambros, V. (1999). Cell cycle-dependent sequencing of cell fate decisions in Caenorhabditis elegans vulva precursor cells. *Development* **126**, 1947-1956.

Arur, S., Ohmachi, M., Nayak, S., Hayes, M., Miranda, A., Hay, A., Golden, A. and Schedl, T. (2009). Multiple ERK substrates execute single biological processes in Caenorhabditis elegans germ-line development. *Proc. Natl. Acad. Sci. USA* **106**, 4776-4781. doi:10.1073/pnas.0812285106

Bengoechea-Alonso, M. T. and Ericsson, J. (2009). A phosphorylation cascade controls the degradation of active SREBP1. *J. Biol. Chem.* **284**, 5885-5895. doi:10.1074/jbc.M807906200

Berset, T., Hoier, E. F., Battu, G., Canevascini, S. and Hajnal, A. (2001). Notch inhibition of RAS signaling through MAP kinase phosphatase LIP-1 during C. elegans vulval development. *Science* **291**, 1055-1058. doi:10.1126/science.1055642

Biondi, R. M. and Nebreda, A. R. (2003). Signalling specificity of Ser/Thr protein kinases through docking-site-mediated interactions. *Biochem. J.* **372**, 1-13. doi:10.1042/bj20021641

Brown, N. R., Noble, M. E. M., Endicott, J. A. and Johnson, L. N. (1999). The structural basis for specificity of substrate and recruitment peptides for cyclin-dependent kinases. *Nat. Cell Biol.* **1**, 438-443. doi:10.1038/15674

Buck, S. H., Chiu, D. and Saito, R. M. (2009). The cyclin-dependent kinase inhibitors, cki-1 and cki-2, act in overlapping but distinct pathways to control cell-cycle quiescence during C. elegans development. *Cell Cycle* **8**, 2613-2620. doi:10.4161/cc.8.16.9354

Burdine, R. D., Branda, C. S. and Stern, M. J. (1998). EGL-17(FGF) expression coordinates the attraction of the migrating sex myoblasts with vulval induction in C. elegans. *Development* **125**, 1083-1093.

Chi, Y., Welcker, M., Hizli, A. A., Posakony, J. J., Aebersold, R. and Clurman, B. E. (2008). Identification of CDK2 substrates in human cell lysates. *Genome Biol.* **9**, R149. doi:10.1186/gb-2008-9-10-r149

Chiariello, M., Gomez, E. and Gutkind, J. S. (2000). Regulation of cyclin-dependent kinase (Cdk) 2 Thr-160 phosphorylation and activity by mitogen-activated protein kinase in late G1 phase. *Biochem. J.* **349**, 869-876. doi:10.1042/bj3490869

Clayton, J. E., van den Heuvel, S. J. L. and Saito, R. M. (2008). Transcriptional control of cell-cycle quiescence during C. elegans development. *Dev. Biol.* **313**, 603-613. doi:10.1016/j.ydbio.2007.10.051

Cohen, P. and Frame, S. (2001). The renaissance of GSK3. *Nat. Rev. Mol. Cell Biol.* **2**, 769-776. doi:10.1038/35096075

de la Cova, C. and Greenwald, I. (2012). SEL-10/Fbw7-dependent negative feedback regulation of LIN-45/Braf signaling in C. elegans via a conserved phosphodegron. *Genes Dev.* **26**, 2524-2535. doi:10.1101/gad.203703.112

de la Cova, C., Townley, R., Regot, S. and Greenwald, I. (2017). A real-time biosensor for ERK activity reveals signaling dynamics during C. elegans cell fate specification. *Dev. Cell* **42**, 542-553.e4. doi:10.1016/j.devcel.2017.07.014

Deng, Y., Luo, K. L., Shaye, D. D. and Greenwald, I. (2019). A screen of the conserved kinome for negative regulators of LIN-12 Negative Regulatory Region ("NRR")-missense activity in Caenorhabditis elegans. *G3 (Bethesda)* **9**, 3567-3574. doi:10.1534/g3.119.400471

Eisenmann, D. M., Maloof, J. N., Simske, J. S., Kenyon, C. and Kim, S. K. (1998). The beta-catenin homolog BAR-1 and LET-60 Ras coordinately regulate the Hox gene lin-39 during Caenorhabditis elegans vulval development. *Development* **125**, 3667-3680.

Espinosa, L., Inglés-Esteve, J., Aguilera, C. and Bigas, A. (2003). Phosphorylation by glycogen synthase kinase-3β down-regulates Notch activity, a link for Notch and Wnt pathways. *J. Biol. Chem.* **278**, 32227-32235. doi:10.1074/jbc.M304001200

Euling, S. and Ambros, V. (1996). Heterochronic genes control cell cycle progress and developmental competence of C. elegans vulva precursor cells. *Cell* **84**, 667-676. doi:10.1016/S0092-8674(00)81045-4

Fantz, D. A., Jacobs, D., Glossip, D. and Kornfeld, K. (2001). Docking sites on substrate proteins direct extracellular signal-regulated kinase to phosphorylate specific residues. *J. Biol. Chem.* **276**, 27256-27265. doi:10.1074/jbc.M102512200

Fay, D. S. and Han, M. (2000). Mutations in cye-1, a Caenorhabditis elegans cyclin E homolog, reveal coordination between cell-cycle control and vulval development. *Development* **127**, 4049-4060.

Ferguson, E. L., Sternberg, P. W. and Horvitz, H. R. (1987). A genetic pathway for the specification of the vulval cell lineages of Caenorhabditis elegans. *Nature* **326**, 259-267. doi:10.1038/326259a0

Fox, P. M., Vought, V. E., Hanazawa, M., Lee, M.-H., Maine, E. M. and Schedl, T. (2011). Cyclin E and CDK-2 regulate proliferative cell fate and cell cycle progression in the C. elegans germline. *Development* **138**, 2223-2234. doi:10.1242/dev.059535

Frame, S., Cohen, P. and Biondi, R. M. (2001). A common phosphate binding site explains the unique substrate specificity of GSK3 and its inactivation by phosphorylation. *Mol. Cell* **7**, 1321-1327. doi:10.1016/S1097-2765(01)00253-2

Frøkjær-Jensen, C., Davis, M. W., Sarov, M., Taylor, J., Flibotte, S., LaBella, M., Pozniakovsky, A., Moerman, D. G. and Jorgensen, E. M. (2014). Random and targeted transgene insertion in Caenorhabditis elegans using a modified Mos1 transposon. *Nat. Meth.* **11**, 529-534. doi:10.1038/nmeth.2889

Gauthier, K. and Rocheleau, C. E. (2017). C. elegans vulva induction: an in vivo model to study epidermal growth factor receptor signaling and trafficking. *Methods Mol. Biol.* **1652**, 43-61. doi:10.1007/978-1-4939-7219-7_3

Grbovic, O. M., Basso, A. D., Sawai, A., Ye, Q., Friedlander, P., Solit, D. and Rosen, N. (2006). V600E B-Raf requires the Hsp90 chaperone for stability and is degraded in response to Hsp90 inhibitors. *Proc. Natl. Acad. Sci. USA* **103**, 57-62. doi:10.1073/pnas.0609973103

Greenwald, I. S., Sternberg, P. W. and Horvitz, H. R. (1983). The lin-12 locus specifies cell fates in Caenorhabditis elegans. *Cell* **34**, 435-444. doi:10.1016/0092-8674(83)90377-X

Hajnal, A., Whitfield, C. W. and Kim, S. K. (1997). Inhibition of Caenorhabditis elegans vulval induction by gap-1 and by let-23 receptor tyrosine kinase. *Genes Dev.* **11**, 2715-2728. doi:10.1101/gad.11.20.2715

Hernandez, M. A., Patel, B., Hey, F., Giblett, S., Davis, H. and Pritchard, C. (2016). Regulation of BRAF protein stability by a negative feedback loop involving the MEK-ERK pathway but not the FBXW7 tumour suppressor. *Cell. Signal.* **28**, 561-571. doi:10.1016/j.cellsig.2016.02.009

Hodeify, R., Tarcsafalvi, A., Megyesi, J., Safirstein, R. L. and Price, P. M. (2011). Cdk2-dependent phosphorylation of p21 regulates the role of Cdk2 in cisplatin cytotoxicity. *Am. J. Physiol. Renal Physiol.* **300**, F1171-F1179. doi:10.1152/ajprenal.00507.2010

Hong, Y., Roy, R. and Ambros, V. (1998). Developmental regulation of a cyclin-dependent kinase inhibitor controls postembryonic cell cycle progression in Caenorhabditis elegans. *Development* **125**, 3585-3597.

Hopper, N. A., Lee, J. and Sternberg, P. W. (2000). ARK-1 inhibits EGFR signaling in C. elegans. *Mol. Cell* **6**, 65-75. doi:10.1016/S1097-2765(05)00001-8

Hydbring, P., Bahram, F., Su, Y., Tronnersjö, S., Högstrand, K., von der Lehr, N., Sharifi, H. R., Lilischkis, R., Hein, N., Wu, S. et al. (2010). Phosphorylation by Cdk2 is required for Myc to repress Ras-induced senescence in cotransformation. *Proc. Natl. Acad. Sci. USA* **107**, 58-63. doi:10.1073/pnas.0900121106

Jacobs, D., Beitel, G. J., Clark, S. G., Horvitz, H. R. and Kornfeld, K. (1998). Gain-of-function mutations in the Caenorhabditis elegans lin-1 ETS gene identify a C-terminal regulatory domain phosphorylated by ERK MAP kinase. *Genetics* **149**, 1809-1822.

Jacobs, D., Glossip, D., Xing, H., Muslin, A. J. and Kornfeld, K. (1999). Multiple docking sites on substrate proteins form a modular system that mediates recognition by ERK MAP kinase. *Genes Dev.* **13**, 163-175. doi:10.1101/gad.13.2.163

Jongeward, G. D., Clandinin, T. R. and Sternberg, P. W. (1995). sli-1, a negative regulator of let-23-mediated signaling in C. elegans. *Genetics* **139**, 1553-1566.

Kamath, R. S., Fraser, A. G., Dong, Y., Poulin, G., Durbin, R., Gotta, M., Kanapin, A., Le Bot, N., Moreno, S., Sohrmann, M. et al. (2003). Systematic functional analysis of the Caenorhabditis elegans genome using RNAi. *Nature* **421**, 231-237. doi:10.1038/nature01278

Kamentsky, L., Jones, T. R., Fraser, A., Bray, M.-A., Logan, D. J., Madden, K. L., Ljosa, V., Rueden, C., Eliceiri, K. W. and Carpenter, A. E. (2011). Improved structure, function and compatibility for CellProfiler: modular high-throughput image analysis software. *Bioinformatics* **27**, 1179-1180. doi:10.1093/bioinformatics/btr095

Karp, X. and Greenwald, I. (2013). Control of cell-fate plasticity and maintenance of multipotency by DAF-16/FoxO in quiescent Caenorhabditis elegans. *Proc. Natl. Acad. Sci. USA* **110**, 2181-2186. doi:10.1073/pnas.1222377110

Kim, W., Underwood, R. S., Greenwald, I. and Shaye, D. D. (2018). OrthoList 2: a new comparative genomic analysis of human and Caenorhabditis elegans genes. *Genetics* **210**, 445-461. doi:10.1534/genetics.118.301307

Kipreos, E. T. and van den Heuvel, S. (2019). Developmental control of the cell cycle: insights from Caenorhabditis elegans. *Genetics* **211**, 797-829. doi:10.1534/genetics.118.301643

Korzelius, J., The, I., Ruijtenberg, S., Portegijs, V., Xu, H., Horvitz, H. R. and van den Heuvel, S. (2011). C. elegans MCM-4 is a general DNA replication and checkpoint component with an epidermis-specific requirement for growth and viability. *Dev. Biol.* **350**, 358-369. doi:10.1016/j.ydbio.2010.12.009

Lackner, M. R. and Kim, S. K. (1998). Genetic analysis of the Caenorhabditis elegans MAP kinase gene mpk-1. *Genetics* **150**, 103-117.

Lavoie, H. and Therrien, M. (2015). Regulation of RAF protein kinases in ERK signalling. *Nat. Rev. Mol. Cell Biol.* **16**, 281-298. doi:10.1038/nrm3979

Lees, E., Faha, B., Dulic, V., Reed, S. I. and Harlow, E. (1992). Cyclin E/cdk2 and cyclin A/cdk2 kinases associate with p107 and E2F in a temporally distinct manner. *Genes Dev.* **6**, 1874-1885. doi:10.1101/gad.6.10.1874

Lents, N. H., Keenan, S. M., Bellone, C. and Baldassare, J. J. (2002). Stimulation of the Raf/MEK/ERK cascade is necessary and sufficient for activation and Thr-160 phosphorylation of a nuclear-targeted CDK2. *J. Biol. Chem.* **277**, 47469-47475. doi:10.1074/jbc.M207425200

Nash, P., Tang, X., Orlicky, S., Chen, Q., Gertler, F. B., Mendenhall, M. D., Sicheri, F., Pawson, T. and Tyers, M. (2001). Multisite phosphorylation of a CDK inhibitor sets a threshold for the onset of DNA replication. *Nature* **414**, 514-521. doi:10.1038/35107009

Nusser-Stein, S., Beyer, A., Rimann, I., Adamczyk, M., Piterman, N., Hajnal, A. and Fisher, J. (2012). Cell-cycle regulation of NOTCH signaling during C. elegans vulval development. *Mol. Syst. Biol.* **8**, 1-14. doi:10.1038/msb.2012.51

Orlicky, S., Tang, X., Willems, A., Tyers, M. and Sicheri, F. (2003). Structural basis for phosphodependent substrate selection and orientation by the SCFCdc4 ubiquitin ligase. *Cell* **112**, 243-256. doi:10.1016/S0092-8674(03)00034-5

Regot, S., Hughey, J. J., Bajar, B. T., Carrasco, S. and Covert, M. W. (2014). High-sensitivity measurements of multiple kinase activities in live single cells. *Cell* **157**, 1724-1734. doi:10.1016/j.cell.2014.04.039

Ritt, D. A., Monson, D. M., Specht, S. I. and Morrison, D. K. (2010). Impact of feedback phosphorylation and Raf heterodimerization on normal and mutant B-Raf signaling. *Mol. Cell. Biol.* **30**, 806-819. doi:10.1128/MCB.00569-09

Saei, A., Palafox, M., Benoukraf, T., Kumari, N., Jaynes, P. W., Iyengar, P. V., Muñoz-Couselo, E., Nuciforo, P., Cortés, J., Nötzel, C. et al. (2018). Loss of USP28-mediated BRAF degradation drives resistance to RAF cancer therapies. *J. Exp. Med.* **215**, 1913-1928. doi:10.1084/jem.20171960

Saito, R. M., Perreault, A., Peach, B., Satterlee, J. S. and van den Heuvel, S. (2004). The CDC-14 phosphatase controls developmental cell-cycle arrest in C. elegans. *Nat. Cell Biol.* **6**, 777-783. doi:10.1038/ncb1154

Sallee, M. D. and Greenwald, I. (2015). Dimerization-driven degradation of C. elegans and human E proteins. *Genes Dev.* **29**, 1356-1361. doi:10.1101/gad.261917.115

Sawa, H. and Korswagen, H. (2013). Wnt signaling in C. elegans. In *WormBook* (ed. The C. elegans Research Community). doi:10.1895/wormbook.1.7.2

Schmitz, C., Kinge, P. and Hutter, H. (2007). Axon guidance genes identified in a large-scale RNAi screen using the RNAi-hypersensitive Caenorhabditis elegans strain nre-1(hd20) lin-15b(hd126). *Proc. Natl. Acad. Sci. USA* **104**, 834-839. doi:10.1073/pnas.0510527104

Sears, R., Nuckolls, F., Haura, E., Taya, Y., Tamai, K. and Nevins, J. R. (2000). Multiple Ras-dependent phosphorylation pathways regulate Myc protein stability. *Genes Dev.* **14**, 2501-2514. doi:10.1101/gad.836800

Seydoux, G., Salvage, C. and Greenwald, I. (1993). Isolation and characterization of mutations causing abnormal eversion of the vulva in Caenorhabditis elegans. *Dev. Biol.* **157**, 423-436. doi:10.1006/dbio.1993.1146

Shin, H. and Reiner, D. J. (2018). The signaling network controlling C. elegans vulval cell fate patterning. *J. Dev. Biol.* **6**, 30. doi:10.3390/jdb6040030

Sternberg, P. W. (2005). Vulval development. In *WormBook* (ed. The C. elegans Research Community). doi:10.1895/wormbook.1.6.1

Sternberg, P. W. and Horvitz, H. R. (1986). Pattern formation during vulval development in C. elegans. *Cell* **44**, 761-772. doi:10.1016/0092-8674(86)90842-1

Stiernagle, T. (2006). Maintenance of C. elegans. In *WormBook* (ed. The C. elegans Research Community). doi:10.1895/wormbook.1.101.1

Sulston, J. E. and Horvitz, H. R. (1977). Post-embryonic cell lineages of the nematode, Caenorhabditis elegans. *Dev. Biol.* **56**, 110-156. doi:10.1016/0012-1606(77)90158-0

Sundaram, M. V. (2013). Canonical RTK-Ras-ERK signaling and related alternative pathways. In *WormBook* (ed. The C. elegans Research Community). doi:10.1895/wormbook.1.80.2

Tan, P. B., Lackner, M. R. and Kim, S. K. (1998). MAP kinase signaling specificity mediated by the LIN-1 Ets/LIN-31 WH transcription factor complex during C. elegans vulval induction. *Cell* 93, 569-580. doi:10.1016/S0092-8674(00)81186-1

Underwood, R. S., Deng, Y. and Greenwald, I. (2017). Integration of EGFR and LIN-12/Notch signaling by LIN-1/Elk1, the Cdk8 kinase module, and SUR-2/Med23 in vulval precursor cell fate patterning in Caenorhabditis elegans. *Genetics* **207**, 1473-1488. doi:10.1534/genetics.117.300192

Wei, W., Jin, J., Schlisio, S., Harper, J. W. and Kaelin, W. G. Jr. (2005). The v-Jun point mutation allows c-Jun to escape GSK3-dependent recognition and destruction by the Fbw7 ubiquitin ligase. *Cancer Cell* **8**, 25-33. doi:10.1016/j.ccr.2005.06.005

Welcker, M., Singer, J., Loeb, K. R., Grim, J., Bloecher, A., Gurien-West, M., Clurman, B. E. and Roberts, J. M. (2003). Multisite phosphorylation by Cdk2 and GSK3 controls cyclin E degradation. *Mol. Cell* **12**, 381-392. doi:10.1016/S1097-2765(03)00287-9

Welcker, M., Orian, A., Grim, J. E., Grim, J. A., Eisenman, R. N. and Clurman, B. E. (2004). A nucleolar isoform of the Fbw7 ubiquitin ligase regulates c-Myc and cell size. *Curr. Biol.* **14**, 1852-1857. doi:10.1016/j.cub.2004.09.083

Welcker, M., Larimore, E. A., Swanger, J., Bengoechea-Alonso, M. T., Grim, J. E., Ericsson, J., Zheng, N. and Clurman, B. E. (2013). Fbw7 dimerization determines the specificity and robustness of substrate degradation. *Genes Dev.* **27**, 2531-2536. doi:10.1101/gad.229195.113

Yada, M., Hatakeyama, S., Kamura, T., Nishiyama, M., Tsunematsu, R., Imaki, H., Ishida, N., Okumura, F., Nakayama, K. and Nakayama, K. I. (2004). Phosphorylation-dependent degradation of c-Myc is mediated by the F-box protein Fbw7. *EMBO J.* **23**, 2116-2125. doi:10.1038/sj.emboj.7600217

Yoo, A. S., Bais, C. and Greenwald, I. (2004). Crosstalk between the EGFR and LIN-12/Notch pathways in C. elegans vulval development. *Science* **303**, 663-666. doi:10.1126/science.1091639

Yumimoto, K. and Nakayama, K. I. (2020). Recent insight into the role of FBXW7 as a tumor suppressor. *Semin. Cancer Biol.* doi:10.1016/j.semcancer.2020.02.017

Zhang, X. and Greenwald, I. (2011). Spatial regulation of lag-2 transcription during vulval precursor cell fate patterning in Caenorhabditis elegans. *Genetics* **188**, 847-858. doi:10.1534/genetics.111.128389

Table S1: *C. elegans* strains used in this study

Click here to Download Table S1

Table S2: *C. elegans* transgenes used in this study

Click here to Download Table S2

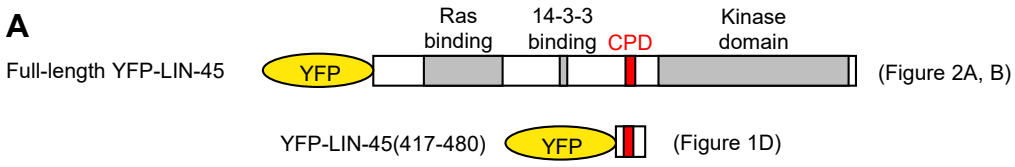

B **LIN-45(417-480) region**

CPD motif

420 430 440 450 460 470 480

TTSSLVAAHLHTLPLTPPQSAPPQKISPGFFRNRSRSPGERLDAQRPRPPQKPHHEDWEILPNE

Alanine substitutions made in YFP-LIN-45(417-480) reporter

		Summary of reporter stability:
TTSSLVAAHLHTLPLAPPQSAPPQKISPGFFRNRSRSPGERLDAQRPRPPQKPHHEDWEILPNE	T432A	Stabilized
TTSSLVAAHLHTLPLTPPQAAPPQKISPGFFRNRSRSPGERLDAQRPRPPQKPHHEDWEILPNE	S436A	Stabilized
TTSSLVAAHLHTLPLTPPQSAAAQKISPGFFRNRSRSPGERLDAQRPRPPQKPHHEDWEILPNE	P438A+P439A	Degraded in P6.p
TTSSLVAAHLHTLPLTPPQSAPPAAISPGFFRNRSRSPGERLDAQRPRPPQKPHHEDWEILPNE	Q440A+K441A	Degraded in P6.p
TTSSLVAAHLHTLPLTPPQSAPPQKAAPGFFRNRSRSPGERLDAQRPRPPQKPHHEDWEILPNE	I442A+S443A	Degraded in P6.p
TTSSLVAAHLHTLPLTPPQSAPPQKISAAFFRNRSRSPGERLDAQRPRPPQKPHHEDWEILPNE	P444A+G445A	Degraded in P6.p
TTSSLVAAHLHTLPLTPPQSAPPQKISPGAARNRSRSPGERLDAQRPRPPQKPHHEDWEILPNE	F446A+F447A	Stabilized

C **Stability of mutant forms of YFP-LIN-45(417-480) reporter: mutation of +0 Thr and +4 Ser**

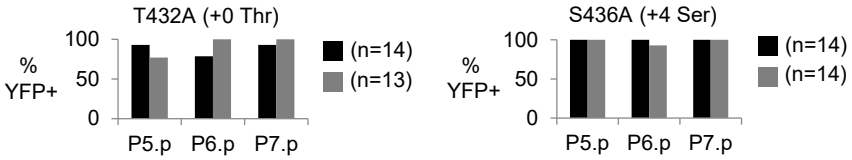

D **Stability of mutant form of YFP-LIN-45(417-480) reporter: alanine scan**

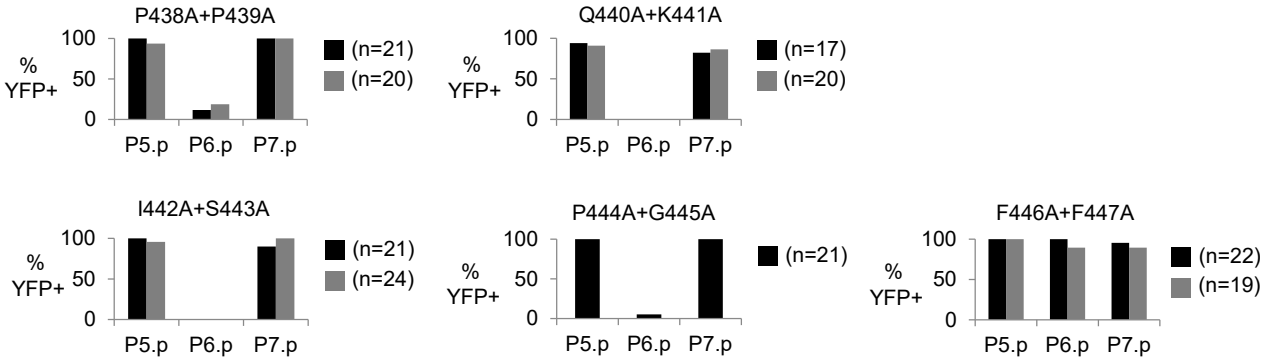

Figure S1. YFP-tagged LIN-45 protein reporters. A) Schematic of full-length YFP-LIN-45 and truncated YFP-LIN-45(417-480) proteins. **B)** Amino acid sequence of LIN-45(417-480) region. The +0 Thr and +4 Ser CPD residues are shown in red. In mutant forms tested, alanine substitutions are shown in blue. **C-D)** Stability of mutant forms of the truncated YFP-LIN-45(417-480) reporter. With exception of the P444A+G445A form, two independent strains were scored for each mutant form tested. Percentage of VPCs with visible YFP fluorescence, and number larvae scored (n) is shown for each strain. (C) Mutations at the +0 Thr or +4 Ser abolish degradation in P6.p. (D) Mutations at F446 and F447 abolish degradation in P6.p.

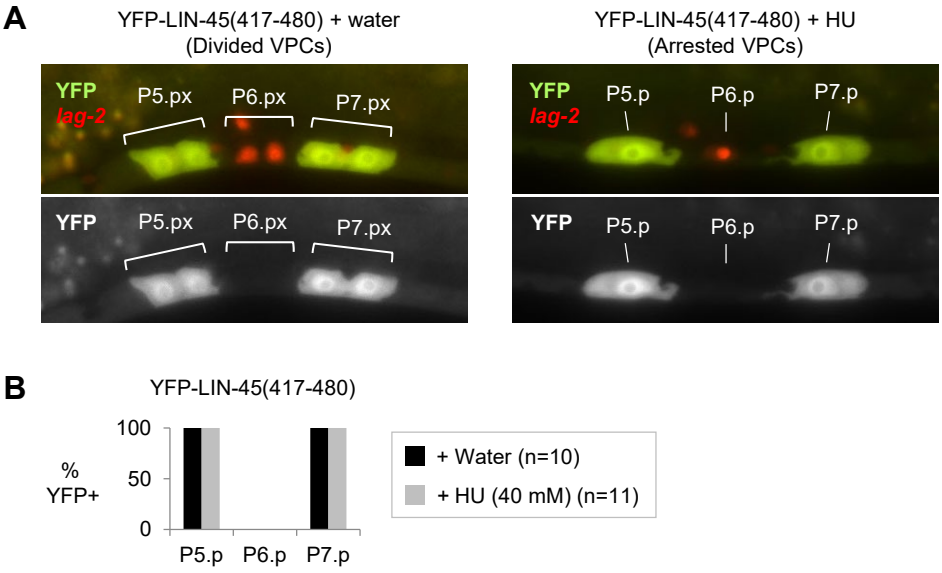

Figure S2. Blockade of S phase does not prevent degradation of the truncated LIN-45(417-480) reporter. Larvae were picked during L2 lethargus based on their lack of locomotion and pharyngeal pumping, transferred to plates with either water (control) or 40 mM hydroxyurea (HU), and grown for 6 hours. At that time, VPCs of all larvae on control plates had divided. For 11/12 larvae grown on HU plates, the VPCs did not divide. We excluded the larva in which VPCs had divided from our analysis. **A)** YFP-tagged LIN-45(417-480) (green) and *arIs222[lag-2p::2xNLS-tagRFP]* (red) proteins in representative images of L3 stage larvae. Top, merged image; bottom, YFP-LIN-45(417-480) alone in grayscale. For the water control, VPCs had divided, and the locations of daughters P5.px, P6.px, and P7.px are indicated with brackets. For the HU-treated larva, undivided VPCs P5.p, P6.p, and P7.p are indicated. **B)** Percentage of VPCs positive for YFP-LIN-45(417-480) in either the water control or HU-treated larvae, and the number of larvae scored (n) is shown.

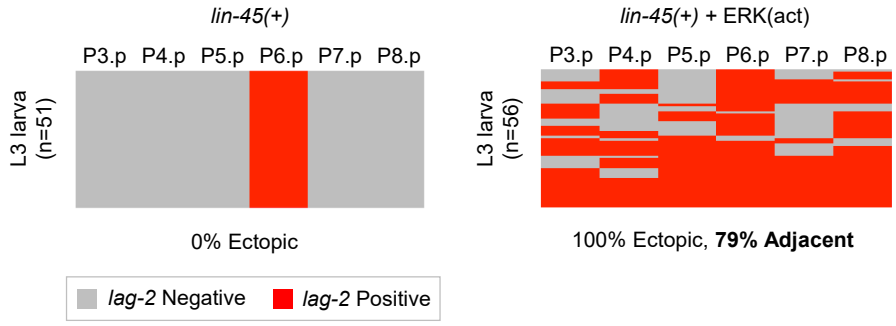

Figure S3. *lag-2* transcription is induced by ERK(act). The *gaIs37* transgene, referred to here as ERK(act), leads to highly active MPK-1/ERK and causes ectopic expression of a transcriptional reporter for *lag-2*, *arIs222[lag-2p::2xNLS-tagRFP],* a direct target of the EGFR-Ras-Raf-ERK signaling pathway and marker of 1° fate. Expression was scored in L3 stage larvae. Each panel represents the *lag-2* positive (red) or negative (gray) status in individual VPCs. Each larva is represented in a row, and VPC is represented in a column. The number of L3 larvae scored (n) is shown at left of each panel. Based on ectopic *lag-2* expression, larvae were categorized as displaying either alternating or adjacent 1° fate. The percentage of larvae that displayed any ectopic 1° fate (% Ectopic), and adjacent 1º fate (% Adjacent) is indicated at each panel.

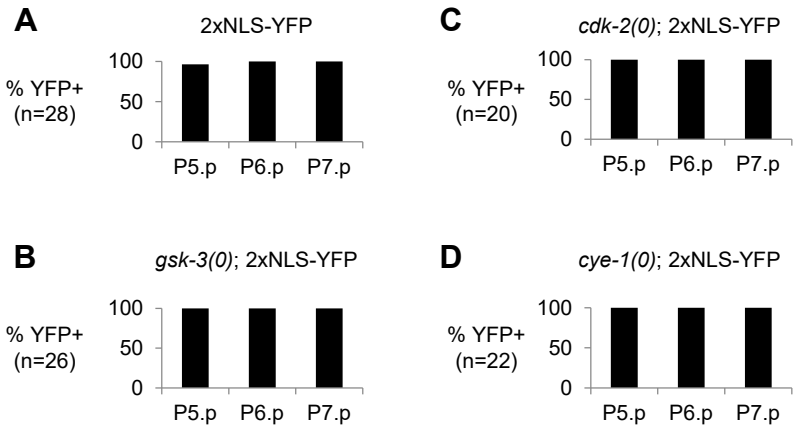

Figure S4. Expression of *lin-31p* is unaffected in *gsk-3*, *cdk-2*, and *cye-1* mutants. In wild-type L3 stage larvae, the *lin-31* promoter (*lin-31p*) is expressed approximately uniformly in P5.p, P6.p, and P7.p. Activity of *lin-31p* was assessed using *arTi88[lin-31p::2xNLS-YFP],* which drives a nuclear-localized YFP. **A)** Percentage of VPCs positive for 2xNLS-YFP in otherwise wild-type larvae, and the number of larvae score (n) is shown. **B-D)** To confirm that the *lin-31p* expression system used to drive YFP-LIN-45 reporters throughout this work is active in the genotypes examined, *arTi88[lin-31p::2xNLS-YFP],* was scored in *gsk-3*, *cdk-2*, and *cye-1* null mutants. Percentage of VPCs positive for 2xNLS-YFP, and the number of larvae scored (n) is shown for (B) *gsk-3(0)* larvae, (C) *cdk-2(0)* larvae, and (D) *cye-1(0)* larvae.